A STUDY OF THE MICROWAVE BRIGHTNESS
TEMPERATURE OF SEA ICE

FINAL REPORT

CONTRACT NO. N00014-85-C-0765

PREPARED FOR

OFFICE OF NAVAL RESEARCH
DEPARTMENT OF THE NAVY
ARLINGTON, VIRGINIA 22217

DTIC
ELECTE
MAR 2 6 1987

A

REPORT No.8362 DECEMBER 1986

*AEROJET
ELECTROSYSTEMS
COMPANY*

AZUSA, CALIFORNIA

87 3 11 112

A STUDY OF THE MICROWAVE BRIGHTNESS TEMPERATURE OF SEA ICE

Final Report

December 1986

Report No. 8362

Contract No. N00014-85-C-0765

by

A. Stogryn

Prepared for

OFFICE OF NAVAL RESEARCH
DEPARTMENT OF THE NAVY
Arlington, Virginia 22217

Prepared by

AEROJET ELECTROSYSTEMS COMPANY
1100 West Hollyvale Street
Azusa, California 91702

INTRODUCTION AND SUMMARY

The work reported here, funded under Contract N00014-85-C-0765, considers the computation of the microwave brightness temperatures of various types of sea ice. The methodology is an application of theoretical and experimental results obtained at Aerojet ElectroSystems Company under previous contracts with the Office of Naval Research. In these studies, the bilocal approximation of strong fluctuation theory was used to develop equations for the effective dielectric constant of both isotropic and anisotropic random media as well as equations for calculating the brightness temperature of isothermal isotropic media. The earlier work also examined the present state of knowledge concerning the dielectric properties of the constituents of sea ice. It was found that there were significant uncertainties relating to the loss tangent of pure ice as well as the dielectric properties of brine in sea ice. The latter problem was overcome by a systematic measurement of the dielectric properties of brine and the derivation of Debye parameters which allow the dielectric constant of brine to be calculated throughout the microwave portion of the electromagnetic spectrum. The uncertainties with respect to the loss tangent of pure ice remain so that a tentative model based on available experimental data must be used.

The specific tasks performed under the present contract consisted of (1) the development of a computer program to calculate the brightness temperature of an isothermal layered structure, each of whose layers could consist of an anisotropic random medium and (2) the application of the model to a variety of sea ice types at different temperatures and the comparison of calculations with some reported measurements. Section 1 of this report

discusses the basic equations required for the computer program and concentrates specifically on the modification of previously reported equations demanded by the introduction of elongated brine cells leading to a description in terms of a tensor correlation function. Section 2 of this report discusses computed brightness temperatures of various types of sea ice. In order to facilitate comparison with experiments, data on new ice, young ice, first year ice and multiyear ice are treated separately. It is found that the main features of the brightness temperature measurements on the first three ice types can be explained by the model over a wide range of temperatures and snow cover conditions. For multiyear ice, however, discrepancies between the theory and experiments begin to appear somewhere in the 20-30 GHz range and become progressively more pronounced at higher frequencies. These appear to be the result of the model underestimating scattering effects on the brightness temperature for multiyear ice and indicates the need for further theoretical developments. Finally, Section 3 contains conclusions and recommendations.

CONTENTS

ILLUSTRATIONS

Section 1

BRIGHTNESS TEMPERATURE OF A RANDOM ANISOTROPIC MEDIUM

Equations for calculating the brightness temperature of an isothermal layered medium have been discussed in [1] for the case where the effective dielectric properties of each of the layers is characterized by a scalar dielectric constant and correlation function. Since it has been shown in [2] that certain forms of sea ice have anisotropic dielectric properties which require a description by means of a second rank dielectric tensor, it is of some interest to see how the basic equations may be generalized to the anisotropic situation. This problem is treated here.

1.1 RELATION OF BRIGHTNESS TEMPERATURE TO SCATTERING COEFFICIENTS

For an isothermal medium there is a close relationship between the brightness temperature and bistatic scattering coefficients, which are proportional to the mean intensity of the scattered field, when the medium is illuminated by a plane electromagnetic wave. Using the relationships developed by Peake [3] and expressing the scattering coefficients of a random medium bounded by flat, parallel surfaces as the sum of a specular term and a bistatic term arising from the random field within the medium, it was shown in [1] that the emissivity of the medium in the direction $-\underline{k}_o$ (see Figure 1-1) corresponding to the polarization p may be expressed as

$$\epsilon_p(\underline{k}_o) = 1 - |R_p|^2 - \frac{1}{4\pi} \int [\gamma_{ph}(\underline{k}_o,\underline{k}) + \gamma_{pv}(\underline{k}_o,\underline{k})] \sin\theta d\theta d\phi \qquad (1)$$

where the integral is evaluated over the upper hemisphere $0 \le \theta \le \pi/2$, $0 \le \phi \le 2\pi$. Here R_p is the reflection coefficient of the medium which, in

the bilocal approximation of strong fluctuation theory, is determined by the effective dielectric constant. The polarization p is customarily taken to be either horizontal (h) or vertical (v) in remote sensing studies so that the scattering coefficients appearing in (1) are of the form $\gamma_{ab}(\underline{k}_o, \underline{k})$ (a,b = h or v) where $\underline{k}_o$ is the propagation vector of the incident plane wave and $\underline{k}$ the propagation vector of the scattered wave in the direction determined by the elementary solid angle $d\Omega = \sin\theta d\theta d\phi$.

With expression (1) for the emissivity, the brightness temperature of the radiation leaving the surface $z = 0$ in the direction $-\underline{k}_o$ and with polarization p is

$$T_p(\underline{k}_o, 0) = \epsilon_p(\underline{k}_o) T_g + |R_p|^2 T_{sky}(\underline{k}_o) + \frac{1}{4\pi} \int [\gamma_{ph} + \gamma_{pv}] T_{sky}(\underline{k}) \sin\theta d\theta d\phi$$

(2)

where T_g is the thermal temperature of the random medium and $T_{sky}(\underline{k})$ is the brightness temperature of the downward flowing radiation arising from the cosmic background radiation as well as the earth's atmosphere and incident on the surface from the direction $-\underline{k}$. Further atmospheric effects arise if the radiometer observing the surface is located at a significant height z above it. These consist of the reduction of $T_p(\underline{k}_o, 0)$ by a transmission factor $L(\underline{k}_o, z)$ and the addition of an upward flowing component of radiation $T_{atm}(\underline{k}_o, z)$ generated by the atmosphere between the surface and the radiometer. Thus the observed brightness temperature is

$$T_p(\underline{k}_o, z) = L(\underline{k}_o, z) T_p(\underline{k}_o, 0) + T_{atm}(\underline{k}_o, z)$$

(3)

The main problem to be addressed in this section is the computation of the reflection coefficient R_p and scattering coefficients γ_{ab} when the random medium is described by a tensor dielectric constant and correlation function appropriate to sea ice as discussed in [2]. The atmospheric effects mentioned above may be treated by standard radiative transfer theory.

1.2 THE REFLECTION COEFFICIENT

According to the bilocal approximation in strong fluctuation theory, the reflection coefficient R_p (p = h or v) in (1) and (2) is determined by the behavior of the mean electric field which, in turn, is dependent on the effective dielectric constant. For sea ice with no preferred azimuthal direction, this is a second rank tensor of the form [2]

$$\underset{\approx}{K} = \begin{pmatrix} K_{11} & 0 & K_{13} \\ 0 & K_{22} & 0 \\ K_{13} & 0 & K_{33} \end{pmatrix} \tag{4}$$

if the incident wave is $\underset{\sim}{k_o} = k_o(\sin\theta_o, 0, -\cos\theta_o)$. Since we consider the problem of a medium located in the region $z < 0$ with air above, (4) holds for $z < 0$ while for $z > 0$, $\underset{\approx}{K}$ is simply the unit dyad $\underset{\approx}{I}$.

Thus, given an electric field

$$\underset{\sim}{E}_{in} = E_o \, \underset{\sim}{\hat{p}} \, \exp[i \, k_o(\sin\theta_o x - \cos\theta_o z)] \tag{5}$$

incident on the medium (see Figure 1-1) from above, the mean field may be expressed as

$$
\underset{\sim}{E}^m = \begin{cases} \underset{\sim}{E}_{in} + R_p\,E_o\,\overset{\wedge}{\underset{\sim}{p}}\,\exp[\,i\,k_o(\sin\theta_o x + \cos\theta_o z)] & \text{if } z > 0 \\ \\ E_o\,\underset{\sim}{f}(z)\,\exp[\,i\,k_o\,\sin\theta_o x] & \text{if } z < 0 \quad (6) \end{cases}
$$

The second summand in the first line of (6) represents the field reflected

in the specular direction while the second line of (6) represents the depth

dependence of the field by the vector $\underset{\sim}{f}(z)$. If a general layered

structure is considered, so that $\underset{\approx}{K}$ in (4) depends on z, an explicit form

for $\underset{\sim}{f}$ cannot be written. However, $\underset{\sim}{f}(z)$ and R_p are determined by the

fact that $\underset{\sim}{E}^m$ is a solution of Maxwell's equations with certain boundary

conditions. Thus $\underset{\sim}{E}^m$ satisfies

$$
\nabla \times \nabla \times \underset{\sim}{E}^m - k_o^2\,\underset{\approx}{K}\,\underset{\sim}{E}^m = 0 \qquad (7)
$$

The boundary conditions require the component of $\underset{\sim}{E}^m$ tangent to the boundary

surface at $z = 0$ be continuous together with the tangential component of

$\nabla \times \underset{\sim}{E}^m$ (which is proportional to the magnetic field). The boundary condi-

tions lead to different results for horizontal and vertical polarization of

the incident wave. Thus, these cases are treated separately.

Considering, first, the case of horizontal polarization, the sym-

metry of the problem requires that $\underset{\sim}{f}$ in (6) be of the form

$$
\underset{\sim}{f}(z) = f(z)\,\overset{\wedge}{\underset{\sim}{h}} \qquad (8)
$$

where $f(z)$ is a scalar valued function. Substitution into (7) shows that

f is determined by the ordinary differential equation

$$\frac{d^2f}{dz^2} + k_o^2[K_{22} - \sin^2\theta_o]\, f = 0 \tag{9}$$

while the boundary conditions lead to the equation

$$\frac{df}{dz} - i\,k_o\,\cos\theta_o\,f = -2i\,k_o\,\cos\theta_o \quad \text{at} \quad z = 0 \tag{10}$$

and the relation

$$R_h = f(0) - 1 \tag{11}$$

It is interesting to note that these equations are the same as those applicable to a scalar dielectric constant [1], [4] with the single exception that the scalar dielectric constant is replaced by the 2,2 component of the dielectric tensor for the anisotropic case.

The situation is more complex for the case of vertical polarization. In this case, the symmetry of the problem requires that $\underset{\sim}{f}(z)$ in (6) have two components:

$$\underset{\sim}{f}(z) = f_x(z)\hat{x} + f_z(z)\,\hat{\underset{\sim}{z}} \tag{12}$$

Upon substituting (12) and (6) in (7) it is found that

$$f_z(z) = \frac{i\,\sin\theta_o}{k_o[K_{33} - \sin^2\theta_o]}\,\frac{d\,f_x}{dz} - \frac{K_{13}}{K_{33} - \sin^2\theta_o}\,f_x \tag{13}$$

and

$$\frac{d^2 f_x}{dz^2} + \frac{1}{K_{33}} \left[-\frac{\sin^2\theta_o}{K_{33} - \sin^2\theta_o} \frac{d K_{33}}{dz} + 2i k_o \sin\theta_o K_{13} \right] \frac{df_x}{dz}$$

$$+ \frac{k_o^2}{K_{33}} \left[K_{11}(K_{33} - \sin^2\theta_o) + \frac{i \sin\theta_o}{k_o} \frac{d K_{13}}{dz} - K_{13}^2 \right.$$

$$\left. - \frac{i \sin\theta_o K_{13}}{k_o(K_{33} - \sin^2\theta_o)} \frac{d K_{33}}{dz} \right] f_x = 0 \tag{14}$$

The boundary conditions require

$$\frac{df_x}{dz} + ik_o \left[-\frac{K_{33} - \sin^2\theta_o}{K_{33} \cos\theta_o} + \frac{K_{13} \sin\theta_o}{K_{33}} \right] f_x = -2ik_o \frac{K_{33} - \sin^2\theta_o}{K_{33}} \quad \text{at} \quad z = 0 \tag{15}$$

together with the equation

$$R_v = 1 - f_x(0)/\cos\theta_o \tag{16}$$

While the derivation of equations (13) - (16) required no approximations beyond those inherent in the bilocal approximation of strong fluctuation theory, they are extremely inconvenient for numerical work because the function $f_x(z)$ is an oscillatory function which must be found over distances of many wavelengths in typical applications to snow-covered sea ice. The numerical techniques discussed in [1] would be useful and applicable except for the possible non-zero values of K_{13} and its derivative. For this reason, these terms will be ignored so that the approximate equations to be solved for vertical polarization are

$$\frac{d^2 f_x}{dz^2} - \frac{\sin^2\theta_o}{K'_{33} - \sin^2\theta_o} \left(\frac{dK'_{33}}{dz}\bigg/ K'_{33}\right)\frac{df_x}{dx} + k_o^2 \frac{K'_{11}}{K'_{33}}(K'_{33} - \sin^2\theta_o) f_x = 0 \tag{17}$$

$$f_z = \frac{i \sin\theta_o}{k_o[K'_{33} - \sin^2\theta_o]} \frac{df_x}{dz} \tag{18}$$

with the boundary condition

$$\frac{df_x}{dx} - i k_o \frac{K'_{33} - \sin^2\theta_o}{K'_{33}\cos\theta_o} f_x = -2i k_o \frac{K'_{33} - \sin^2\theta_o}{K'_{33}} \tag{19}$$

at $z = 0$. Here K'_{11} and K'_{33} are slightly modified values of K_{11} and K_{33}. The discussion below treats the validity of this approximation and the fact that K_{11} and K_{33} should be modified when K_{13} is ignored.

With equations (8) - (11) for horizontal polarization and (16) - (19) for vertical polarization, the numerical problems for a multi-layered anisotropic structure are exactly the same as those treated for the isotropic case in [1]. Thus, the specification of the mean field and reflection coefficients for both horizontal and vertical polarization may be considered completed when the components of the dielectric tensor are given. For sea ice, these are discussed in [2].

The nature of the hypothesis that K_{13} may be ignored for the case of vertical polarization will now be examined. To do this notice that, according to the analysis in [2], the equation (4) may be written more generally as

$$\underset{\approx}{K} = A \underset{\approx}{I} + B \underset{\sim}{k} \underset{\sim}{k} + C \underset{\sim}{z} \underset{\sim}{z} + D(\underset{\sim}{k}\underset{\sim}{z} + \underset{\sim}{z}\underset{\sim}{k}) \tag{20}$$

where the scalar coefficients A, B, C, and D depend only on $\underset{\sim}{k} \cdot \underset{\sim}{z}$ and k^2. For frazil or multiyear ice which, according to the model in [2], are characterized by an isotropic mean structure, the coefficients C and D are exactly equal to zero. But then the analysis in [5] shows that for transverse waves the coefficient B has no influence on the effective dielectric constant so that $\underset{\approx}{K}$ may be treated as equal to the scalar A. Thus, for frazil and multiyear ice, no approximation is made at all. For all types of ice, no approximation is made at $\theta_o = 0$ because it was shown in [2] that $K_{13} = 0$ whenever $k_x = 0$. There is an approximation, however, for other angles for anisotropic ice forms. In order to treat this case, consider a uniform medium without gradients so that $f_x(z)$ in (12) has an exponential z dependence $\exp[-ik_z z] = \exp[-ik_o(K-\sin^2\theta_o)z]$ where K is the effective dielectric constant appropriate to θ_o. If it is required that k_z be equal to the exact propagation constant (i.e., obtained as in [2] without neglecting K_{13}) then by substituting the exponential into (7) and specifying that

$$K'_{11} = K_{22} \tag{21}$$

it is found that K'_{33} must be given by

$$K'_{33} = \frac{\sin^2\theta_o \, K_{22}}{K_{22} + \sin^2\theta_o - K} \tag{22}$$

Thus, a procedure has been found for modifying the dielectric constants which does not change the propagation constant of the wave when K_{13} is ignored.

However, there is a change in the ratio $f_z(z)/f_x(z)$ which is induced by this approach. From (18), the approximate ratio is

$$f_z/f_x = \frac{\sin\theta_o\sqrt{K-\sin^2\theta_o}}{K'_{33} - \sin^2\theta_o} \tag{23}$$

while from (13) the exact ratio is

$$f_z/f_x = \frac{\sin\theta_o\sqrt{K-\sin^2\theta_o} - K_{13}}{K_{33} - \sin^2\theta_o} \tag{24}$$

Numerical comparisons for a variety of anisotropic ice parameters and angles θ_o show that (23) yields values close to (24). The largest differences occur for high salinities and temperatures near 0°C where differences of the order of 10% in both the real and imaginary parts of the ratios were found for large θ_o and frequencies near 20 GHz. At frequencies below 10 GHz and above 30 GHz, the error is significantly less. Computations from (23) and (24) are nearly identical for low ice temperatures and/or low salinity. Thus, it is seen that the approximation in the dielectric constant for vertical polarization of the incident wave leads to acceptably small errors in the ratio f_z/f_x while preserving the magnitude and direction of the propagation constant of the electromagnetic wave.

1.3 SCATTERING COEFFICIENTS

The computation of the scattering coefficients for sea ice follows the pattern discussed in [4]. The essential difference is that the scalar correlation function is replaced by a fourth rank correlation tensor describing the anisotropic inhomogeneities. This adds a number of new terms to the scattering coefficients Y_{ab} (a,b = h or v).

Specifically, the random electric field $\underset{\sim}{\mathbf{E}}^r$ in the bilocal approximation of strong fluctuation theory obeys the equation (see [4] and the required substitutions mentioned in [6] to convert the results of [4] to strong fluctuation theory)

$$\nabla \times \nabla \times \underset{\sim}{\mathbf{E}}^r - k_o^2 \underset{\approx}{\mathbf{K}}_o \underset{\sim}{\mathbf{E}}^r = -\underset{\approx}{\xi} \underset{\sim}{\mathbf{E}}^m \tag{25}$$

where $\underset{\approx}{\mathbf{K}}_o$ is the diagonal quasi-static dielectric tensor

$$\underset{\approx}{\mathbf{K}}_o = \text{diag} (K_{01}, K_{01}, K_{03}) \tag{26}$$

discussed in [2] for sea ice. In (25), $\underset{\approx}{\xi}$ is the random second rank tensor

$$\underset{\approx}{\xi} = \Delta\underset{\approx}{\mathbf{L}}[\underset{\approx}{\mathbf{I}} + \underset{\approx}{\mathbf{S}} \Delta\underset{\approx}{\mathbf{L}}]^{-1} \tag{27}$$

where $\underset{\approx}{\mathbf{S}}$ is the coefficient of the delta function in the Green's function for the operator on the left-hand side of (25) and

$$\Delta\underset{\approx}{\mathbf{L}} = k_o^2(\underset{\approx}{\mathbf{K}}_o - \underset{\approx}{\mathbf{K}}^r) \tag{28}$$

Here, $\underset{\approx}{\mathbf{K}}^r$ is the local dielectric constant (i.e., corresponding to air or an ice grain which contains brine cells).

Proceeding as in [4], the expected value $\left\langle \mathbf{E}_i^r(\underset{\sim}{\mathbf{r}})\mathbf{E}_j^{r*}(\underset{\sim}{\mathbf{r}}) \right\rangle$ (where the * indicates complex conjugate) may be formed in terms of an integral over the Green's function. After a decomposition which represents the expected

value as an angular spectrum of random waves $E_i^r(\underline{k})$ propagating in the

direction $\underline{k}$ (see Figure 1-1), it is found that

$$\left\langle E_i^r(\underline{k})E_j^{r*}(\underline{k})\right\rangle = (2\pi)^{-2} E_0^2 k_0^2 \cos\theta \int_{-\infty}^{0} dz' \int_{-\infty}^{0} dz'' A_{ik}(z',\underline{k}) A_{jm}^*(z'',\underline{k})$$

$$f_\ell(z') f_n^*(z'') W_{k\ell mn}'(k_{ox} - k_x, k_y, z',z'') \qquad (29)$$

where the summation convention is used for repeated Latin letter indices, the

tensor $\underset{\approx}{A}$ is the two-dimensional Fourier transform of the Green's function

exactly as in [4], $\underline{f}$ is the vector (6) describing the mean electric field

in the medium, and the fourth rank tensor W' is the Fourier transform

$$W_{k\ell mn}'(\xi,\eta,z',z'') = \int_{-\infty}^{0} dxdy\, C_{k\ell mn}'(x,y,z',z'') \exp[i(\xi x+\eta y)] \qquad (30)$$

of the correlation tensor

$$C_{k\ell mn}'(x,y,z',z'') = \left\langle \xi_{k\ell}(x + x', y + y', z') \xi_{mn}^*(x', y', z'')\right\rangle \qquad (31)$$

which is an even function of x and y. Finally, the scattering coeffi-

cients are related to (29) by [4]

$$Y_{ab}(\underline{k}_o,\underline{k}) = (4\pi\cos\theta/E_0^2 \cos\theta_o)\, b_i\, b_j \left\langle E_i^r(\underline{k})\, E_j^{r*}(\underline{k})\right\rangle \qquad (32)$$

To obtain practical expressions for Y_{ab}, it is necessary to

specify the symmetry of the tensors $\underset{\approx}{A}$ and W' in more detail. In the

case of the Green's function, the physical situation under consideration is azimuthally symmetric. Just as in [4], this implies that $\underset{\approx}{A}$ is of the form

$$
\underset{\approx}{A} = \begin{pmatrix} A_{\phi\phi} + \cos^2\phi(A_{\rho\rho}-A_{\phi\phi}) & \cos\phi\,\sin\phi\,(A_{\rho\rho}-A_{\phi\phi}) & \cos\phi A_{\rho z} \\ \cos\phi\,\sin\phi\,(A_{\rho\rho}-A_{\phi\phi}) & A_{\phi\phi}+\sin^2\phi(A_{\rho\rho}-A_{\phi\phi}) & \sin\phi A_{\rho z} \\ \cos\phi\,A_{z\rho} & \sin\phi\,A_{z\rho} & A_{zz} \end{pmatrix} \tag{33}
$$

Further, since the Green's function is a solution of the vector wave equation, the relations

$$
A_{z\rho} = -\tan\theta\,A_{\rho\rho} \tag{34}
$$

$$
A_{zz} = -\tan\theta\,A_{\rho z} \tag{35}
$$

are found to hold so that there are only three independent functions $A_{\phi\phi}$, $A_{\rho\rho}$, and $A_{\rho z}$ which need to be evaluated. These will be considered in more detail later. For the present, we turn to the tensors $C'_{ijk\ell}$ and $W'_{ijk\ell}$ in order to be able to reduce (32) to a manageable form.

It should be noted that $C'_{ijk\ell}$ differs from $C_{ijk\ell}$ defined in [2] for sea ice only by the fact that the complex conjugate is used in the second factor on the right-hand side of (31). Thus, using the corresponding assumptions regarding an exponential correlation for air bubbles with a correlation length ℓ_a and volume fraction v_{air} and grains of ice with correlation length ℓ_g and volume fraction v_g, one can immediately write

$$C'_{ijk\ell}(r_2-r_1) = [\xi_{airij}\xi^*_{airk\ell} + \overline{\xi}_{gij}\overline{\xi}^*_{gk\ell} - \xi_{airij}\overline{\xi}^*_{gk\ell} - \overline{\xi}_{gij}\xi^*_{airk\ell}]$$

$$v_{air}(1 - v_{air}) \exp[-|r_2-r_1|/\ell_a$$

$$+ B'_{ijk\ell}(0) \exp[-|r_2-r_1|/\ell_g] \qquad (36)$$

where

$$B'_{ijk\ell}(0) = [\overline{\xi_{gij}\xi^*_{gk\ell}} - \overline{\xi}_{gij}\overline{\xi}^*_{gk\ell}] v_{grain} \qquad (37)$$

The notation of [2] is used. The most important immediate fact concerning (36) is that $C'_{ijk\ell}$ and, hence, its Fourier transform $W'_{ijk\ell}$ have the same symmetry as $C_{ijk\ell}$ (and $B_{ijk\ell}(0)$) in [2] with the exception that the symmetry under the interchange $(ij) \longleftrightarrow (k\ell)$ is lost. That is, they are invariant under orthogonal transformations leaving the z-axis fixed and are symmetric in the first two indices and last two indices. Hence, it is possible to write

$$W'_{ijk\ell} = a'_1 \delta_{ij} \delta_{k\ell} + a'_2[\delta_{ik} \delta_{j\ell} + \delta_{i\ell} \delta_{jk}]$$

$$+ b'_1 \delta_{ij} \delta_{k3} \delta_{\ell3} + b'_2[\delta_{ik} \delta_{j3} \delta_{\ell3} + \delta_{i\ell} \delta_{j3} \delta_{k3}$$

$$+ \delta_{jk} \delta_{i3} \delta_{\ell3} + \delta_{j\ell} \delta_{i3} \delta_{k3}] + b'_3 \delta_{k\ell} \delta_{i3} \delta_{j3}$$

$$+ c' \delta_{i3} \delta_{j3} \delta_{k3} \delta_{\ell3} \qquad (38)$$

where the coefficients are scalars. Since C' is an even function of x_2-x_1 and y_2-y_1 , (30) and (31) show that

$$W'^*_{k\ell ij} = W'_{ij k\ell} \qquad (39)$$

Thus, using (38), it is found that a'_1 , a'_2 , b'_2 and c' are real while $b'^*_1 = b'_3$. Furthermore, choosing particular values for the indices shows that the coefficients in (38) are related to W' by

$$W'_{1122} = a'_1$$

$$W'_{1212} = a'_2$$

$$W'_{1133} = a'_1 + b'_1$$

$$W'_{1313} = a'_2 + b'_2$$

$$W_{3333} = a'_1 + 2a'_2 + b'_1 + b'^*_2 + 4b'_2 + c' \qquad (40)$$

which, with the exception of W'_{1133} , are real. This set of equations is easily inverted to yield

$$a'_1 = W'_{1122}$$

$$b'_1 = W'_{1133} - W'_{1122}$$

$$a'_2 = W'_{1212}$$

$$b'_2 = W'_{1313} - W'_{1212}$$

$$c' = W'_{3333} - 2\text{Re } W'_{1133} + W'_{1122} - 4W'_{1313} + 2W'_{1212} \qquad (41)$$

With the above equations for the structure of the Green's function and Fourier transform of the correlation tensor, it is a straightforward but lengthy calculation to evaluate (32) for the four combinations of the incident and scattered radiation polarizations of interest. It is found that, in terms of the functions f, f_x, and f_z previously introduced for the mean field,

$$\gamma_{hh} = \left(\frac{k_o^2 \cos^2\theta}{\pi \cos\theta_o}\right)\int dz' \, dz'' \, A_{\phi\phi}(z') \, A_{\phi\phi}^*(z'') \, f(z') \, f^*(z'')$$

$$[(W_{1122}' + W_{1212}') \cos^2\phi + W_{1212}'] \tag{42}$$

$$\gamma_{hv} = \left(\frac{k_o^2}{\cos\theta_o}\right) \int dz' \, dz'' \, f(z') \, f^*(z'') \left\{ A_{\rho\rho}(z') \, A_{\rho\rho}^*(z'') \right.$$

$$[(W_{1122}' + W_{1212}') \sin^2\phi + W_{1212}']$$

$$\left. + A_{\rho z}(z') \, A_{\rho z}^*(z'') \, W_{1313}' \right\} \tag{43}$$

$$\gamma_{vh} = \left(\frac{k_o^2 \cos^2\theta}{\cos\theta_o}\right)\int dz' \, dz'' \, A_{\phi\phi}(z') \, A_{\phi\phi}^*(z'') \left\{ f_x(z') \, f_x^*(z'') \right.$$

$$[(W_{1122}' + W_{1212}') \sin^2\phi + W_{1212}'] \left. + f_z(z') \, f_z^*(z'') \, W_{1313}' \right\}$$

$$\tag{44}$$

$$\gamma_{vv} = \left(\frac{k_o^2}{\cos\theta_o}\right) \int dz'\, dz'' \left\{ A_{\rho\rho}(z')\, A_{\rho\rho}^*(z'')\, f_x(z')\, f_x^*(z'') \right.$$

$$[(W'_{1122} + W'_{1212})\cos^2\phi + W'_{1212}]$$

$$+ \cos\phi[W'_{1133}\, A_{\rho\rho}(z')\, A_{\rho z}^*(z'')\, f_x(z')\, f_z^*(z'')$$

$$+ W'_{1133}\, A_{\rho\rho}^*(z'')\, A_{\rho z}(z')\, f_x^*(z'')\, f_z(z')]$$

$$+ W'_{3333}[A_{\rho\rho}(z')\, A_{\rho\rho}^*(z'')\, f_z(z')\, f_z^*(z'')$$

$$+ A_{\rho z}(z')\, A_{\rho z}^*(z'')\, f_x(z')\, f_x^*(z'')$$

$$+ \cos\phi\, A_{\rho\rho}(z')\, A_{\rho z}^*(z'')\, f_x^*(z'')\, f_z(z')$$

$$\left. + \cos\phi\, A_{\rho\rho}^*(z'')\, A_{\rho z}(z')\, f_x(z')\, f_z^*(z'')] \right\} \tag{45}$$

Upon comparison with the corresponding isotropic, scalar case treated in [4], quite a few additional terms are found. These terms arise from the anisotropic tensor nature of the correlation function. Even for the special cases of frazil and old ice, where the correlation tensor is invariant under arbitrary orthogonal transformations, there is a difference from the case of a scalar correlation function for not only a'_1, but also a'_2 do not vanish in (40) and (41). The true scalar case, where a'_2 also vanishes, would require that the ice grains be described by a scalar dielectric constant or, equivalently, in terms of the model in [2], that the brine cells be spherical rather than elongated in shape. Fortunately, although there are additional terms for all types of sea ice, the z' and z'' dependence of the integrals will be of the form treated in [1] from the point of view of numerical evaluation provided that the depth dependence of the

of the Green's function and correlation tensor are of the same nature as in

[1]. It will be shown below that this is indeed the case so that computer

codes based on the same numerical scheme are applicable. Of course, they

will be considerably longer because of the new terms.

1.4   GREEN'S FUNCTIONS

The Green's function $\underset{\approx}{\Gamma}(\underset{\sim}{r},\underset{\sim}{r}')$ to be used in computing the scatter-

ing coefficients is defined as the solution of the equation

$$\nabla \times \nabla \times \underset{\approx}{\Gamma} - k_o^2 \underset{\approx}{K}_o \underset{\approx}{\Gamma} = \underset{\approx}{I} \delta(\underset{\sim}{r} - \underset{\sim}{r}') \tag{46}$$

where $\underset{\approx}{K}_o$ is the quasi-static dielectric tensor (26). If the Fourier

transform

$$\Gamma_{ij} = (2\pi)^{-2} \int_{-\infty}^{\infty} d\xi \int_{-\infty}^{\infty} d\eta \; a_{ij}(z,z',\xi,\eta) \; \exp\left\{i[\xi(x-x')+\eta(y-y')]\right\} \tag{47}$$

is introduced, then the tensor $\underset{\approx}{A}$ in (33) is defined in terms of the value

at $z = 0$ of a_{ij} for the special values of the transform variables

$$\xi = k_o \sin\theta \cos\phi$$

$$\eta = k_o \sin\theta \sin\phi \tag{48}$$

as in [4]. Explicit differential equations for a_{ij} are found by substitut-

ing (47) into (46). Since the symmetry of a_{ij} is exactly the same as that

of A_{ij}, the three independent functions describing $\underset{\approx}{A}$ are readily found to

be defined by the following. For $A_{\phi\phi}$:

$$A_{\phi\phi}(z',\underline{k}) = a_{\phi\phi}(0) \tag{49}$$

where

$$\frac{d^2 a_{\phi\phi}}{dz^2} + k_o^2(K_{01} - \sin^2\theta)\, a_{\phi\phi} = -\delta(z - z') \tag{50}$$

and

$$\frac{da_{\phi\phi}}{dz} - i\, k_o\cos\theta\, a_{\phi\phi} = 0 \quad \text{at} \quad z = 0 \tag{51}$$

For $A_{\rho\rho}$:

$$A_{\rho\rho}(z',\underline{k}) = a_{\rho\rho}(0) \tag{52}$$

where

$$\frac{d^2 a_{\rho\rho}}{dz^2} - \frac{\sin^2\theta}{K_{03}(K_{02} - \sin^2\theta)}\frac{dK_{03}}{dz}\frac{da_{\rho\rho}}{dz} + k_o^2\frac{K_{01}}{K_{03}}(K_{03} - \sin^2\theta)a_{\rho\rho}$$

$$= -\frac{K_{03} - \sin^2\theta}{K_{03}}\,\delta(z - z') \tag{53}$$

and

$$\frac{da_{\rho\rho}}{dz} - i\, k_o\, \frac{K_{03} - \sin^2\theta}{K_{03}\, \cos\theta}\, a_{\rho\rho} = 0 \quad \text{at} \quad z = 0 \tag{54}$$

For $A_{\rho z}$:

$$A_{\rho z}(z',k) = a_{\rho z}(0) \tag{55}$$

where

$$\frac{d^2 a_{\rho z}}{dz^2} - \frac{\sin^2\theta}{K_{03}(K_{03} - \sin^2\theta)}\frac{dK_{03}}{dz}\frac{da_{\rho z}}{dz} + k_o^2\frac{K_{01}}{K_{03}}(K_{03} - \sin^2\theta)a_{\rho z}$$

$$= \frac{i\,\sin\theta}{k_o\, K_{03}}\left[-\frac{d\,\delta(z - z')}{dz} + \frac{1}{K_{03} - \sin^2\theta}\frac{dK_{03}}{dz}\delta(z - z')\right] \tag{56}$$

and

$$\frac{da_{\rho z}}{dz} - \frac{i\, k_o(\kappa_{03} - \sin^2\theta)}{\kappa_{03}\,\cos\theta}\, a_{\rho z} = -\frac{i\,\sin\theta}{k_o\,\kappa_{03}}\,\delta(z') \quad \text{at} \quad z = 0 \qquad (57)$$

In all cases the boundary condition as $z \rightarrow -\infty$ is that $\underset{\approx}{A}$ be an outgoing wave.

While slightly more complicated than the corresponding equations for the isotropic case where the dielectric constant is a scalar, these equations are still of the same mathematical form as treated in [1]. Thus, equivalent Riccati equations may be introduced and solved numerically as discussed in [1].

1.5   CORRELATION FUNCTION

The only remaining problem to be discussed in connection with the computation of the scattering coefficients is the treatment of the Fourier transform of the correlation tensor (31). The first step is the computation of the Fourier transforms of the two exponential functions in (36). Letting

$$V_\ell(\xi,\eta,z,z') = \int_{-\infty}^{\infty} dx \int_{-\infty}^{\infty} dy \, \exp[-|\underline{r}-\underline{r}'|/\ell]\, \exp[-i(\xi(x-x')+\eta(y-y')) \qquad (58)$$

when ℓ may be either of the correlation lengths ℓ_a or ℓ_g in (36), it is seen that $W'_{k\ell mn}(k_{ox}-k_x,k_y,z',z'')$ in (29) has a $\underline{k}_o,\underline{k}$, and spatial dependence defined by the functions $V_\ell(k_{ox}-k_x,k_y,z,z')$ ($\ell = \ell_a$ or ℓ_g). The integral in (58) may be evaluated explicitly to yield

$$V_\ell = 2\pi\ell^2\, u^{-3}[1 + u|z - z'|/\ell]\, \exp[-u|z - z'|/\ell] \qquad (59)$$

where

$$u = [1 + \ell^2(\xi^2 + \eta^2)]^{1/2} \tag{60}$$

Thus, upon using (36) and (37), the components of W' occurring in (42) – (45) may be expressed as

$$W'_{1122} = B'_{1122}(0) \, v_{\ell g} + |\xi_{air} - \overline{\xi}_{g11}|^2 \, v_{air}(1 - v_{air}) \, V_{\ell a} \tag{61}$$

$$W'_{1212} = B'_{1212}(0) \, v_{\ell g} \tag{62}$$

$$W'_{1133} = B'_{1133}(0) \, v_{\ell g} + (\xi_{air11} - \overline{\xi}_{g11})(\xi^*_{air33} - \overline{\xi}^*_{g33}) \, v_{air}(1 - v_{air}) v_{\ell a} \tag{63}$$

$$W'_{1313} = B'_{1313}(0) \, v_{\ell g} \tag{64}$$

$$W'_{3333} = B'_{3333}(0) \, v_{\ell g} + |\xi_{air33} - \overline{\xi}_{g33}|^2 \, v_{air}(1 - v_{air}) \, V_{\ell a} \tag{65}$$

The remainder of the problem is identical to the evaluation of the tensor $C_{ijk\ell}$ in [2]. Approximations have to be made when the probability of the orientation of the ice grains has a preferred direction just as in [2]. For frazil and old ice, where all solid angles are equally probable, a more exact computation is possible. Since the details of the computation are lengthy, but follow that in [2] (differing only in the occurrence of terms containing complex conjugates), only the results will be given. Both ξ_{air} and the components of the tensor $\underset{\approx}{\overline{\xi}}_g$ are the same as in [2] so that only the tensor B' needs to be described. Using the notation of [2], for all cases except for frazil and old ice,

$$B'_{1122}(0) = \left\{ \frac{1}{4}\left|\frac{S_3\beta^2\cos\theta_B\sin^2\theta_B}{\alpha_1\gamma}\right|^2 - \mathrm{Re}\left(\bar{\xi}_{g11}\frac{S_3\beta^2\cos^2\theta_B\sin^2\theta_B}{\alpha_1\gamma}\right) \right.$$

$$\left. - \frac{1}{8}\left|\frac{\beta\sin^2\theta_B[\alpha_3+S_3\beta]}{\alpha_1\gamma}\right|^2 \right\} v_{grain} \tag{66}$$

$$B'_{1212}(0) = \frac{1}{8}\left|\frac{\beta\sin^2\theta_B[\alpha_3+S_3\beta]}{\alpha_1\gamma}\right|^2 v_{grain} \tag{67}$$

$$B'_{1313}(0) = \frac{1}{2}\left|\frac{\beta\cos\theta_B\sin\theta_B}{\gamma}\right|^2 v_{grain} \tag{68}$$

$$B'_{1133}(0) = B'_{3333}(0) = 0 \tag{69}$$

where θ_B is the mean angle between the axes of the brine cells and the vertical. In the case of frazil and old ice,

$$B'_{1212}(0) = B'_{1313}(0) = \frac{1}{15}\left|\frac{\beta}{\gamma}\right| v_{grain} \tag{70}$$

$$B'_{1122}(0) = B'_{1133}(0) = \frac{1}{3}[B'_{ijji}(0) - 12B'_{1212}(0)] \tag{71}$$

$$B'_{3333}(0) = B'_{1122}(0) + 2B'_{1212}(0) \tag{72}$$

where the doubly contracted term in (71) is given by

$$B'_{ijji}(0) = \left\{ \mathrm{Tr}(\underset{\approx}{P}\ \underset{\approx}{P}*) - \frac{1}{3}\mathrm{Tr}\ \underset{\approx}{P} \right\} v_{grain} \tag{73}$$

Here, the second rank tensor $\underset{\approx}{P}$ is the diagonal tensor

$$\underset{\approx}{P} = \text{diag} \left(\frac{k_o^2(K_{of}-K_1)}{1 + k_o^2 S_f(K_{of}-K_1)} \quad , \quad \frac{k_o^2(K_{of}-K_1)}{1 + k_o^2 S_f(K_{of}-K_1)} \quad , \right.$$

$$\left. \frac{k_o^2(K_{of}-K_3)}{1 + k_o^2 S_f(K_{of}-K_3)} \right) \tag{74}$$

and Tr mean trace.

References for Section 1

[1]   A. Stogryn, "A study of the microwave brightness temperature of

        snow from the point of view of strong fluctuation theory," IEEE

        Trans. Geosc. Remote Sens., GE-24, pp 220-231 (1986).

[2]   A. Stogryn, "An analysis of the tensor dielectric constant of sea

        ice at microwave frequencies," Aerojet Electrosystems Co., Report

        7975, Oct 1985, prepared for the Office of Naval Research under

        Contract N00014-83-C-0726.

[3]   W. Peake, "Interaction of electromagnetic waves with some natural

        surfaces," IRE Trans. Ant. and Prop., AP-7, pp S324-S329 (1959).

[4]   A. Stogryn, "Electromagnetic scattering by random dielectric

        constant fluctuations in a bounded medium," Radio Science, 9,

        pp 509-185 (1974).

[5]   A. Stogryn, "The bilocal approximation for the effective dielectric

        constant of an isotropic random medium," IEEE Trans. Ant. and Prop.,

        AP-32, pp 517-520 (1984).

[6]   A. Stogryn, "The bilocal approximation for the electric field in

        strong fluctuation theory," IEEE Trans. Ant. and Prop., AP-33,
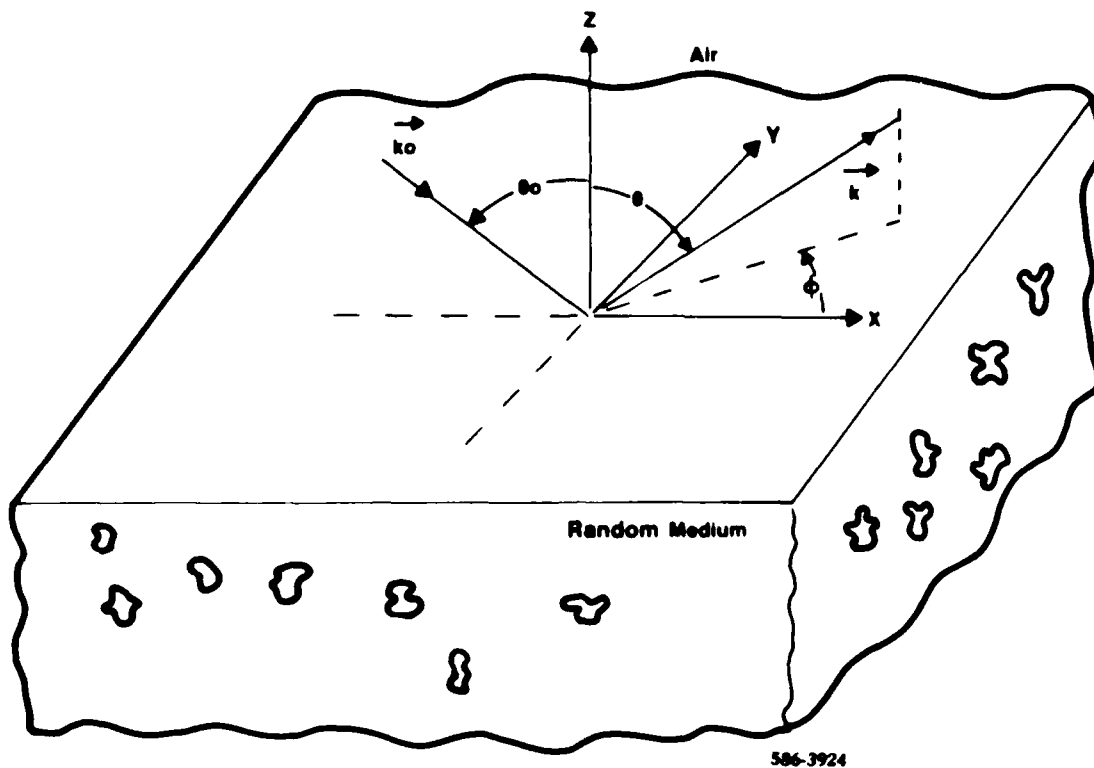
        pp 985-986 (1983).

Figure 1-1. Geometry for Brightness Temperature Computation

Section 2

THE BRIGHTNESS TEMPERATURE OF SEA ICE

The theory developed in Section 1 may be applied to the computation of the brightness temperature of various types of sea ice. It will be seen that it leads to predictions of microwave brightness temperature signatures that do not necessarily fall neatly into the categories which have been developed by the World Meteorological Organization (WMO) for the visual identification of ice types. A difficulty of this nature has also been noted in [1] where a comparison of the ice types distinguishable by the radiometric observations discussed in [1] is shown not to discriminate between young ice and first-year ice. A different classification was proposed in [1] (see Table 2-1). This classification still has an element of dependence on ice thickness. However, the computations based on the theory of this report indicate that the deciding factors determining the microwave signature are, except for the very thinnest of ice covers (of the order of 1 cm thickness where the underlying sea water may influence the signature), thickness independent. The critical factors are the ice salinity and the presence or absence of snow cover for new, young, and first-year ice. The conventional WMO categories, however, will be retained here in order to facilitate comparisons with published results. New, young, first-year and multiyear sea ice are discussed below.

2.1 NEW ICE

Although reports on the microwave brightness temperature of sea ice have appeared in the literature since 1972 [2] and distinguished between "old" and "new" ice, a more systematic classification of the "new" ice category

occurred only in later studies. Several recent observations of new ice have been reported in the literature. These include those of the NORSEX Group [3], Hollinger, et al [1], and Troy, et al [4]. Before examining the results of these particular experiments, it will be useful to make some observations on the physical characteristics of sea ice from its formation to the beginning of the melting season.

A very useful description of these characteristics is given by Nakawo and Sinha [5]. They observed ice at Pond Inlet, Canada from freeze-up through May with a careful documentation of salinity profiles, temperature, and snow cover. An important observation from the point of view of microwave radiometric studies was that the initial salinity of the ice after formation can be extremely high. For example, a value of 25°/oo was measured in one case and the authors commented that even this may not be the upper bound because of possible brine drainage during the removal of the core from the ice sheet. This initial salinity drops very rapidly to a more stable value. In the example cited, the salinity had dropped to 8.5°/oo within a week. Afterwards, it remained relatively constant with a tendency to decrease slowly during the rest of the season. The air temperature was generally below -20°C during these measurements. For warmer days, one would expect the high initial salinity to drop even faster because of the enhanced brine drainage. The growth rate of the ice depends, of course, on the air tempera-ture. Typical rates ranged from about 0.7 to 1.7 cm/day for the temperatures prevailing at Pond Inlet (-20 to -40°C except during a warmer period in the first few weeks). The snow cover, which will be of interest below, was also monitored. Within a few weeks of the freeze-up the snow cover was already about 8 cm thick and throughout the remainder of the season it fluctuated

around 11.4 ±4.2 cm. The snow density was 0.35 ±0.04 g/cm³ during most of the season in agreement with earlier reported results. However, it was mentioned that the density may have been lower than this during the early growth period.

Turning to the microwave observations, the NORSEX results [3] will be considered first. The observations were made between the end of September and early October 1979. The ice temperature was of the order of -1°C. Measurements at frequencies of 4.9, 10.4, 21, 36 and 94 GHz with both vertical and horizontal polarization were made at a nominal angle of incidence $\theta = 50°$ (this varied by about ±3° due to heeling of the shipboard platform). Figure 2-1 is a plot of the deduced emissivity (i.e., after removing atmospheric effects and dividing by assumed ice temperature of 272 K) of the calm sea near the ice together with newly frozen pancake ice (case C in Figure 4 of [3]) for both horizontal and vertical polarization. The computed sea water emissivity is also shown and is mainly of interest as a check on the atmospheric correction procedure and the calibration of the instruments since the radiometric behavior of sea water is relatively well understood. Computed values, assuming an ice density $\rho = 0.9$ g/cm³, a salinity S = 12.3°/oo, frazil (i.e., random ice grain orientations in the theory of Section 1) with a mean air bubble diameter $d_a = 0.5$ mm and a grain diameter $d_g = 4$ mm, and no snow cover, are also shown for an angle of incidence $\theta = 50°$. The agreement is quite good. Although the salinity of the ice was not stated in [3], the assumed value appears to be reasonable on the basis of the warm temperatures and the discussion above. Computations (not shown) were also performed for columnar ice with a mean brine cell angle from the vertical of 24°. In this case, a salinity of 13°/oo (which is still quite reasonable)

had to be assumed in order to obtain a fit to the experimental data which is roughly as good as that shown for frazil. For columnar ice, S = 12.3⁰/oo yields a distinctly poorer fit to the data. In view of the fact that the uppermost layer of ice is generally frazil or randomly oriented columnar ice [1], [6], the initial assumption is probably more realistic although the microwave evidence does not indicate a distinct preference for one or the other of these models. The underlying sea water has almost no effect on the computed emissivity for an ice thickness of 1 cm because of the high attenuation through the ice. Thus, for all practical purposes, the ice thickness has no direct bearing on the emissivity. A characteristic feature of these results is the monotonic increase of the emissivity with increasing frequency. This can be traced directly to the fact that at this high salinity and high temperature, both of which imply a large brine volume, the dielectric constant of the sea ice is quite large at the lower frequencies but gradually decreases as the frequency increases.

For the warm ice temperatures under the NORSEX conditions one would expect rapid surface desalinization and, perhaps, a lowering of the ice surface density due to brine drainage as the ice develops. Thus, it is not surprising that for the densely packed 3 cm thick pancake ice (case D in Figure 4 of [3]) the emissivity is considerably higher than for the thin pancake ice. Figure 2-2 is a plot of this data together with computations which assumed an ice density ρ = 0.8 g/cm^3, salinity S = 9.3⁰/oo, mean air bubble diameter d_a = 0.5 mm, and mean grain size d_q = 4 mm. Again, no preferred orientation of the ice grains is assumed although, with an adjustment of the salinity, similar results are obtained for columnar ice with a mean brine cell angle of 24°. It is seen that while the computations for

2-4

vertical polarization agree well with the measurements, they are too low for horizontal polarization. There does not seem to be a ready explanation for this discrepancy. As in the case of thin pancake ice, both theory and experiment show the same characteristic increase of emissivity with increasing frequency.

Another set of data on snow-free new ice is found in [1] where nadir-viewing ($\theta = 0°$) measurements were made at frequencies of 19, 22, 31, and 90 GHz during the freeze-up period in October 1981. The ice temperature was approximately 270 K during the experiments. Figure 2-3 is a comparison of the experimental data (together with an indication of the range of observed values) with computations which assume randomly oriented ice grains in ice with $\rho = 0.85$ g/cm^3, $d_a = 0.5$ mm, $d_g = 4$ mm and a number of different salinities. These parameters were not measured in the aircraft measurements program. However, increasing the density to 0.9 g/cm^3 reduces the computed emissivities slightly. It is seen that the computations generally fall within the measured range but that the higher frequency data fall on the lower salinity curves. This is quite plausible since the smaller penetration depth of the higher frequencies would emphasize conditions closest to the surface where some brine has probably drained out. No attempt was made to model this situation because there is no data available on salinity gradients within a centimeter of the surface. It should be noticed that an increase of emissivity with increasing frequency occurs in this data just as in the NORSEX experiments although the magnitude of the change is smaller. This is due to the lower brine volumes resulting from the lower temperature.

Data on new ice at much lower temperatures is given in [4] where nadir viewing ($\theta = 0°$) measurements at 14, 19, 31, and 90 GHz were made during

April 1977. The ice temperature ranged between 261 and 264 K. An assumed ice temperature of 263 K was used in the computations shown in Figure 2-4. It is seen that, except for 90 GHz, the data tend to follow a curve with high density and very high salinity. This is entirely reasonable considering the time of year. The ice will be classified as new only for a short period because of the rapid growth to be expected so that possibly very high salinities could arise as pointed out above. The exception at 90 GHz could be accounted for by a desalinization of a very thin surface layer. Again, there is a characteristic increase in emissivity with increasing frequency which is due to the decrease of the dielectric constant with increasing frequency.

Before leaving the subject of new ice, some observations will be made on a possible model for new and young ice which has been mentioned several times in the literature (see e.g., [1], [3], [4]). It is suggested that these types of ice have a thin film of water on the surface. Model computations have been made for new ice covered with a film of brine with salinity high enough to prevent freezing and with thickness ranging from 0.007 to 0.1 mm. The results are shown in Figure 2-5 at nadir for $\rho = 0.9$ g/cm^3, S = 10°/oo and T_g = 270 K and in Figure 2-6 for $\rho = 0.9$ g/cm^3, S = 10.3°/oo, and T_g = 263 K. These should be compared with Figures 2-3 and 2-4 respectively. Considering Figure 2-5 first, it is seen that a film of brine with a thickness of the order of 4 to 20 micrometers would be required to explain the observations below 31 GHz but, for the assumed ice salinity of 10°/oo cannot explain the measurements at 90 GHz. However, just as for the computations of Figure 2-3, if it is assumed that a lower ice salinity exists near the surface layer which affects 90 GHz, the computed emissivity at 90 GHz can be raised slightly. For S = 6°/oo, the emissivity at 90 GHz

becomes 0.900 for a film thickness of 4 micrometers but only 0.888 for a film thickness of 10 micrometers. This is still significantly below the measured value and below the value 0.912 achieved at 90 GHz for the film-free case in Figure 2-3. It is not known if the required film thickness below 40 GHz are reasonable. No measurements exist, but the required values do seem to be small. Similar comments may be made concerning Figure 2-6 where a film thickness of the order of 20 to 50 micrometers is required to explain the data below 31 GHz but causes difficulty at 90 GHz. Upon reducing S to 6°/oo not much improvement is obtained because the low temperature already implies a low brine volume. Increasing the salinity to 20°/oo reduces the required film thickness to about 20 micrometers up to 31 GHz but again results in an emissivity value which is much too low at 90 GHz. In view of the fact that high frequency data in all cases would be difficult to explain if a film were present, it is probable that this model is not correct. Rather new and young ice will feel moist to the touch simply because the high salinity will lead to high brine volumes in the ice. This is a volume, not a surface effect.

2.2   YOUNG ICE

Both [1] and [4] present data on young ice observed at nadir from an aircraft. The emissivity behaves differently in the two experiments. While the emissivity data in [4] basically shows the monotonic increasing behavior with increasing frequency discussed for new ice, the data in [1] has a somewhat higher, almost frequency independent emissivity that is indistin-guishable from that of first year ice (to be discussed below). While the ice temperatures differed in the two cases, this does not appear to be the source of the differences. Rather, the presence of a thin layer of wet snow in the ice observed in [1] seems to account for the difference.

Figure 2-7 is a plot of the relevant data. Measurements from [1] are for an ice temperature of 270 K. There was very little snow on the young ice at the time of the overflights but detailed ground truth data at Mould Bay on the young ice during the time of the overflights showed that the ice was covered with 3.2 to 6 cm of snow with a bottom layer of wet snow whose thickness ranged from 1 to 3.5 cm. Details of the volume fraction of water in the snow and its density were not published in [1] but it was indicated that at several sites the bottom layer was slush while at other sites it was not fully saturated. For the computations, it was assumed that volume fractions of water v_w = 2 and 3% (far from being slush) existed in the bottom layer and that the snow density was 0.35 g/cm^3. Considering the time of day of the measurements, the top layer could have had a very small amount of free water. It was assumed that v_w ranged from 0.5% to 0.8% in this layer. Computations were averaged for a number of total and bottom layer thicknesses in the stated range and assuming a mean snow grain diameter of 1 mm. As for the underlying ice, the grains were assumed to have no preferred orientation. The other ice parameters were ρ = 0.85 g/cm^3 , S = 10.9°/oo, mean air bubble diameter d_a = 0 ⁻ mm, and mean grain size d_g = 4 mm. It is seen that the average of the computations yield a generally high emissivity which deviates by at most 0.01 from a mean value of slightly more than 0.95. There is little systematic frequency dependence in the computations. Of course, by changing the snow and ice parameters somewhat, one could obtain slightly different average values than those shown. One should compare these results with Figure 2-3 which shows roughly the same ice conditions but without snow cover. The effect of the snow is to raise the emissivity considerably and to

flatten the frequency response curve. The former effect of snow on ice has often been pointed out in the literature. For the snow-free young ice discussed in [4], the ice temperatures ranged from 256 to 260 K. A value of 258 K was assumed in the computations together with the same ice parameters as above except that the salinity was allowed to vary. The computed results, which tend to reproduce the data, are considerably lower than for the 270 K data and look very much like the computations shown for new ice in Figures 2-3 and 2-4. The main difference is a shift to higher emissivities which is readily understandable on the basis of the lower ice temperature and hence lower brine volume.

2.3   FIRST-YEAR ICE

There are two data sets for first-year ice that will be examined here. First, consider the NORSEX results [3] where the ice temperature was a warm 272 K, but the first-year ice was covered with snow. As was mentioned in the discussion of new ice, both vertically and horizontally polarized brightness temperatures were measured for an angle of incidence $\theta = 50°$. The NORSEX data for first-year ice is shown in Figure 2-8 where, except for the 4.9 GHz and to a much smaller extent the 10.4 GHz data, not much frequency dependence is evident in the emissivity. Model computations for the two polarizations were averaged over 8, 10, and 12 cm depths of snow (a range was chosen since the snow depth was not specified) and a small range of angles near 50° to simulate the angular uncertainty in the NORSEX data. This procedure also had the advantage of averaging over some angular structure which arose in the models due to the plane parallel layered nature of the snow model being investigated. Of course, in actual experiments, one does not

expect to find layered structures whose thickness over a radiometric foot-print is constant to within a fraction of a centimeter. As for the snow conditions, one should expect some moisture in the snow layer nearest the ice (recall the ground truth measurements for warm conditions mentioned for Mould Bay in the previous section) both because of the warm temperature and the fact that salt from the highly saline ice will infiltrate the nearest snow layer thus allowing free water to form in the snow. Hence, computations were performed where the bottom 1 or 2 cm of snow were wet with a volume fraction of 9 to 10% free water. However, the bulk of the snow (7 to 9 cm thick) was allowed to be either dry or with a very small amount of free water (0.5%) to simulate, perhaps, a trace of melting due to solar radiation. In all cases, the snow density was assumed to be 0.35 g/cm^3. The ice conditions were assumed to be $\rho = 0.85$ g/cm^3, $S = 10.9^o/oo$, $d_a = 0.5$ mm, $d_g = 4$ mm and no preferred orientation for the grain axes in the uppermost part of the ice. Computations for the two assumed snow conditions are shown in Figure 2-8. Considering the uncertainties in the assumed conditions, it is seen that the computations are reasonably close to the measurements with the case where the upper snow layer has a trace of free water being slightly better than the dry upper layer.

Much colder first-year ice (T_g = 25(to 257 K) was measured at nadir in the aircraft program described in [4]. The data are shown in Figure 2-9 together with the results of computations with two different snow cover models, both at a temperature T_g = 253 K. The lower curve represents average values for dry snow with a range of thicknesses up to 9.5 cm, a density of 0.35 g/cm^3 and mean grain sizes of 0.7 and 1 mm. The upper curve represents

an average for a layered snow model with a volume fraction of free water v_w = 1 or 2% in the bottom layer of thickness ranging from 2 to 2.5 cm to simulate possible infiltration of salt into the snow and an upper layer with a trace of free water (v_w = 0.5%) to represent possible effects of solar radiation. The total snow thickness for this situation ranged from 9 to 12.5 cm and, again, the density was taken to be 0.35 g/cm^3. The ice in both cases was assumed to have an upper layer of frazil with ρ = 0.85 g/cm^3, d_a = 0.5 mm and d_g = 4 mm. For the dry snow over ice cases, the ice salinity was 10.9°/oo, but was reduced slightly to 10°/oo for the second set of snow conditions. The model with a trace of water yields emissivities closer to the measurements, but there is no independent information to support the assumptions made. Considering the expanded scale and lack of definitive knowledge of snow conditions, the agreement of the measurement and computations in Figure 2-9 is reasonably good. The principal cause for possible concern is the tendency for the computed emissivities to fall somewhat faster with frequency than the measurements above 20 GHz. A possible reason for this is the fact that the loss tangent of the ice grains in the snow at the low temperatures prevailing here is not well known at these frequencies. Since this has an influence on the computed scattering from the snow, the computations are somewhat uncertain. Increasing the loss tangent would raise the computed emissivity at high frequencies.

2.4 MULTIYEAR ICE

The emission characteristics of multiyear ice have been discussed since the earliest microwave observations of sea ice. Usually, no finer distinctions concerning the ice age is made but occasionally, as in [1], second-year ice is separated from older ice. In the present discussion, all multiyear ice is treated as one kind of ice not only because of a lack of

microwave data over a wide range of conditions but also because a clear

delineation of differences in the physical structure of various age subdivi-

sions is not available.

First consider relatively cold multiyear ice such as observed in

[4] in the temperature range 247-256 K at nadir. This may be supplemented

by the data of Gloersen, et al [7] for ice at 250 K, Campbell, et al [8] for

ice in the 257-260 K range, and Gloersen, et al [9] for ice near 260 K. Figure

2-10 is a plot of the measured nadir emissivities in the frequency range below

40 GHz. No indication of the variability was given in [7] and [9], but it is

reasonable to expect the same variability as indicated in [4] and [8]. Snow

was always present on the multiyear ice but details were not given in any of

the reports. For the computations, ice with two basic types of snow cover

were investigated. The first was a uniform dry snow layer in the 14-17 cm thick-

ness range with a density of 0.35 g/cm^3 and mean grain diameter of 1 mm. In

some cases a 1 to 2 mm thick crust with a density of 0.5 g/cm^3 and 1 mm mean

grain diameter was added. The second type of snow cover was a multilayered

snow structure based on the description of snow cover given in [10]. A

covering of snow with two random fresh water ice layers embedded in the snow

was assumed. Of the 14 computed cases, the top, middle, and bottom snow

layers had mean thicknesses and standard deviations from the mean of 4.31

±0.12, 3.07 ±0.27 and 8.90 ±1.3 cm while the two ice layers had mean thick-

nesses and standard deviations of 7.35 ±0.98 and 4.37 ±0.96 mm leading to a

mean snow-ice cover thickness of 17.5 cm on the sea ice. The snow had a

density of 0.35 g/cm^3 and mean grain diameter of 1 mm while the fresh water

ice had a density of 0.9 g/cm^3 with a 0.1 mm mean air bubble diameter. The

old sea ice in both the random and nonrandom snow cover cases was assumed to

2-12

have a density $\rho = 0.6$ g/cm^3 near the surface, salinity $S = 0.01°/oo$, a mean air bubble diameter $d_a = 1$ mm, and a mean grain size $d_q = 4$ mm. The temperature was set equal to 253 K for all of the computations. Average emissivity values for the two distinct snow cover models are shown in Figure 2-10. The random layering leads to a lower emissivity than the uniform snow cover model. Also, a detailed examination of the cases in the first snow model (not shown separately in the figure) shows that a crust on the snow tends to lower the emissivity slightly. Considering the fact that the true physical state of the snow cover is unknown, the computations are seen to reproduce the main features of the measurements to a frequency of about 30 GHz. Above 30 GHz, the computations begin to show an increase with frequency and at 90 GHz average emissivity values of 0.915 and 0.860 for the uniform and random snow cover models are found. These are somewhat higher than the value 0.81 ± 0.04 reported in [4]. Although the computations appear to be too high at 90 GHz, it is interesting to note that particular samples of data discussed in [4] show that there may be an increase in the emissivity of multiyear ice between 31 and 90 GHz. Thus, at least qualitatively the upturn predicted by the theory at high frequencies is confirmed. However, the results in [1], which are considered next, indicate that the increase in emissivity does not begin until a much higher frequency is reached.

The old ice in [1], observed at a temperature $T_g \approx 270$ K, was characterized as second-year, multiyear and old shorefast ice. The old shorefast ice had emissivity values lying between the second-year and multiyear ice and will not be considered further here. Figure 2-11 is a plot of the measurements and shows that the multiyear ice has a consistently lower

emissivity than the second-year ice. Computations using exactly the same sea ice and snow conditions as discussed for Figure 2-10 except that the thermal temperature is raised to $T_g = 270$ K are also shown in Figure 2-11. Again, the true state of the snow cover is not known. Although the frequency range of the measured data is not as large as shown in Figure 2-10, one can see a general agreement between the computations and the data at least to a frequency of 22 GHz. The computations are too high at 31 GHz for the multiyear ice but not for the second-year ice. At 90 GHz, the computed emissivities are definitely higher (0.927 for the uniform snow cover) than the measured values for either the second or multiyear ice types (0.84 and 0.67 respectively).

One may conclude from these examples that the theory is able to account for, in a quantitative fashion, the general decrease in the emissivity of multiyear ice to a frequency somewhere in the 20-30 GHz range. The theory overestimates the emissivity of multiyear ice at higher frequencies. There are two probable reasons for this discrepancy. First, the effect of the snow cover is not being computed correctly because the lack of knowledge of the true loss tangent of dry snow. This is more important than in the case of first-year ice because of the lower emissivity of the underlying multiyear ice compared to first-year ice. Second, and probably more important, is the fact that the theory requires an expansion in a small parameter. Truncating the expansion after the leading scattering terms, as in the bilocal approximation, underestimates the effect of scattering and hence overestimates the emissivity of the underlying sea ice (and, perhaps, snow cover). The agreement between the computations and measurements at lower frequencies is a result of the fact that scattering is less important at lower frequencies so that the truncation is valid.

References for Section 2

[1]   J. Hollinger, B. Troy, R. Ramseier, K. Asmus, M. Hartman, and

        C. Luther, "Microwave emission from high Arctic sea ice during

        freeze-up," J. Geophys. Res., $\underline{89}$ (C5), pp 8104-8122 (1984).

[2]   T. Wilheit, W. Nordberg, J. Blinn, W. Campbell, and A. Edgerton,

        "Aircraft measurements of microwave emission from Arctic sea ice,"

        Remote Sensing of Environment, $\underline{2}$, pp 129-139 (1972).

[3]   NORSEX Group, "Norwegian remote sensing experiment in a marginal

        ice zone," Science, $\underline{220}$, pp 781-787 (1983).

[4]   B. Troy, J. Hollinger, R. Lerner, and M. Wisler, "Measurement of

        the microwave properties of sea ice at 90 GHz and lower frequencies,"

        J. Geophys. Res. $\underline{86}$ (C5), pp 4283-4289 (1981).

[5]   M. Nakawo and N. Sinha, "Growth rate and salinity profile of first-

        year sea ice in the high Arctic," J. Glaciol. $\underline{27}$, pp 315-330 (1981).

[6]   M. Vant, R. Ramseier, and V. Makios, "The complex dielectric con-

        stant of sea ice at frequencies in the range 0.1 - 40 GHz,"

        J. Appl. Phys. $\underline{49}$, pp 1264-1280 (1978).

[7]   P. Gloersen, H. Zwally, A. Chang, D. Hall, W. Campbell, and

        R. Ramseier, "Time-dependence of sea ice concentration and multi-

        year ice fraction in the Arctic basin," Bound. Layer Meteor., $\underline{13}$,

        pp 339-357 (1977).

[8]   W. Campbell, M. Vant, R. Weaver, A. Redmond, L. Arsenault,

        R. Ramseier, H. Zwally, T. Wilheit, T. Chang, D. Hall, L. Gray,

        D. Meeks, M. Bryon. F. Barath, C. Elachi, F. Leberl, and T. Farr,

        "Microwave remote sensing of sea ice in the AIDJEX main experiment,

        Boundary Layer Meteor. $\underline{13}$, pp 309-337 (1978).

References for Section 2 (Continued)

[9]   P. Gloersen, W. Nordberg, T. Schmugge, T. Wilheit, and W. Campbell, "Microwave signatures of first-year and multiyear ice," J. Geophys. Res. 78, pp 3564-3572 (1973).

[10]   C. Mätzler, R. Ramseier, and E. Svendsen, "Polarization effects in sea-ice signatures," IEEE J. Oceanic Eng., OE-9, pp 333-338 (1984).

TABLE 2-1. SEA ICE CLASSIFICATION

Selected WMO Terminology

General	Specific	Ice Thickness	Microwave Classification [1]
New Ice	frazil,grease,slush, shuga,ice rind,nilas	<5 - 10 cm	new ice
Young Ice	gray	10-15 cm	first-year ice
	gray-white	15-30 cm	
First-Year Ice	thin	30-70 cm	
	medium	70-120 cm	
	thick	>120 cm	
Old Ice	second-year ice	up to 2.5 m or more	second-year ice
	multiyear ice	up to 3 m or more	multiyear ice
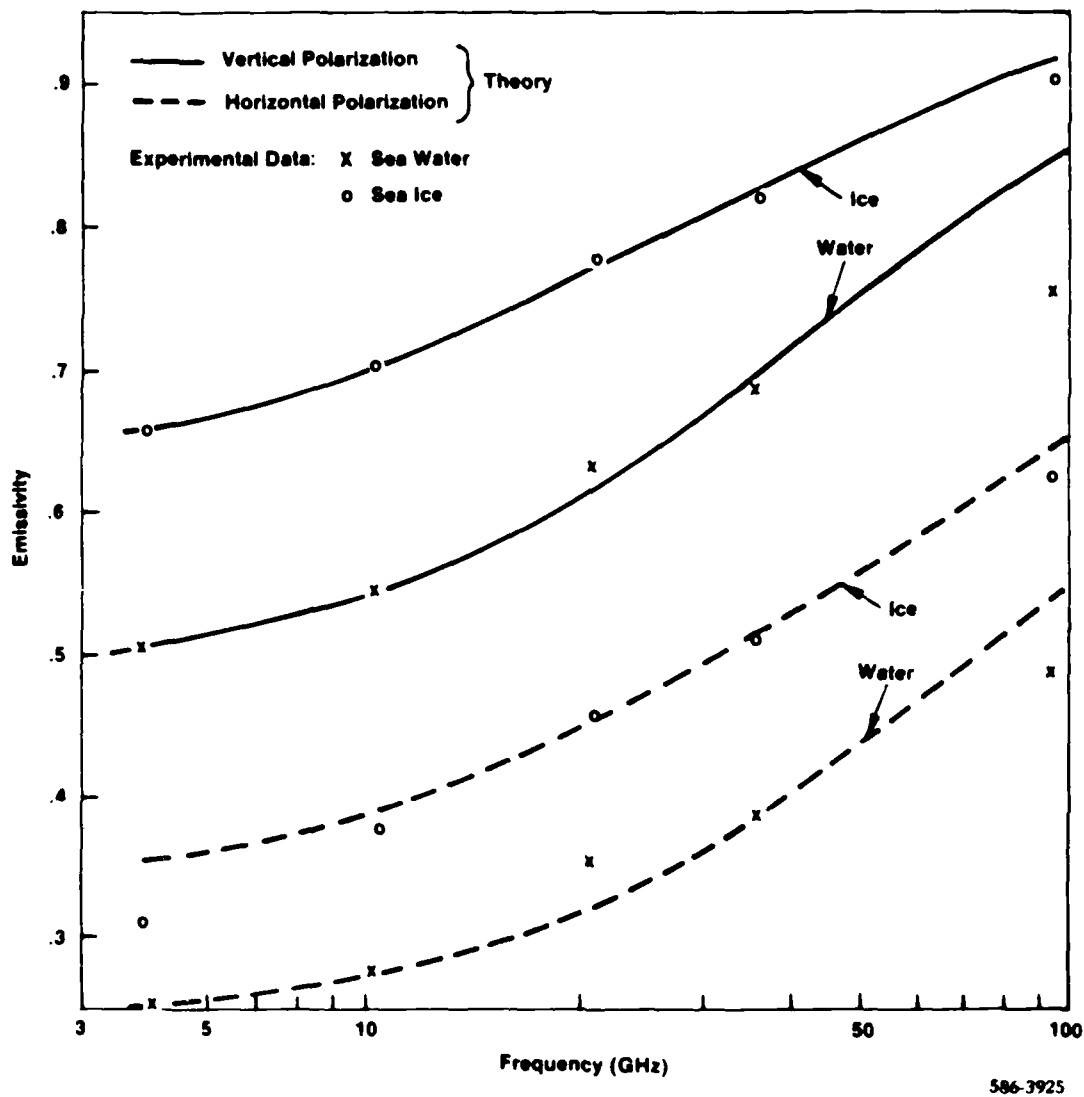
586-3925

Figure 2-1. Emissivity of Sea Water and Thin Pancake Ice as a
Function of Frequency for

$\theta = 50°$ (T_g = 272 K, S = 12.3°/oo, ρ = .9 g/cm³)
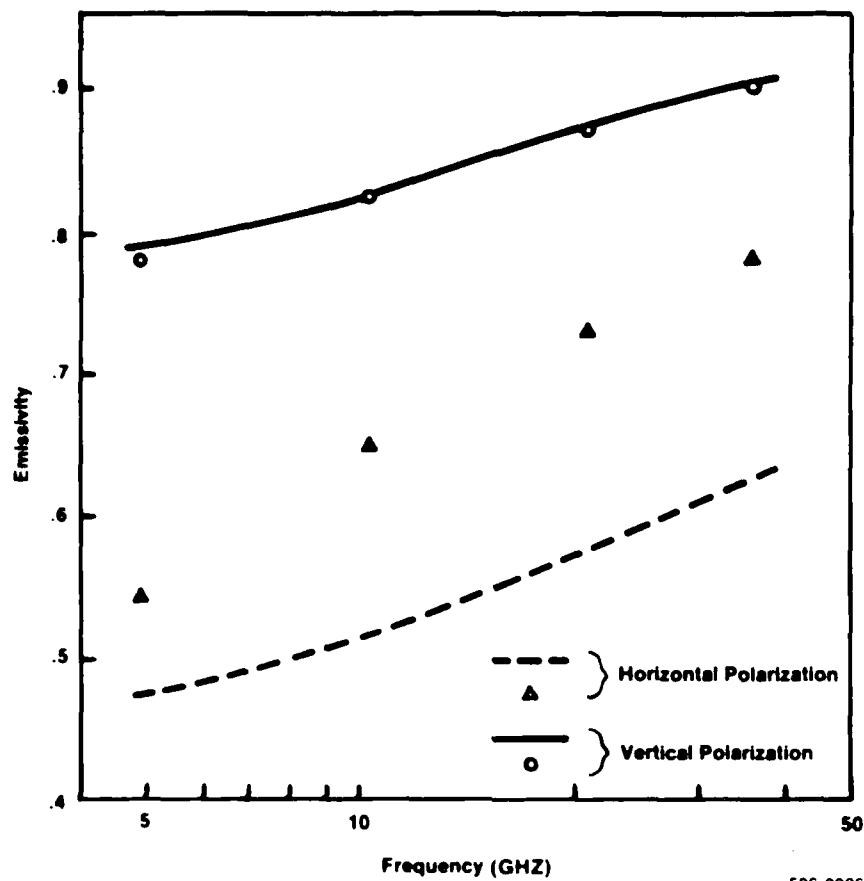
Figure 2-2.   Emissivity of 3 cm Thick Pancake Ice as a
Function of Frequency for

$\theta = 50°$ (T_g = 272 K, S = 9.3°/oo, ρ = .8 g/cm^3)
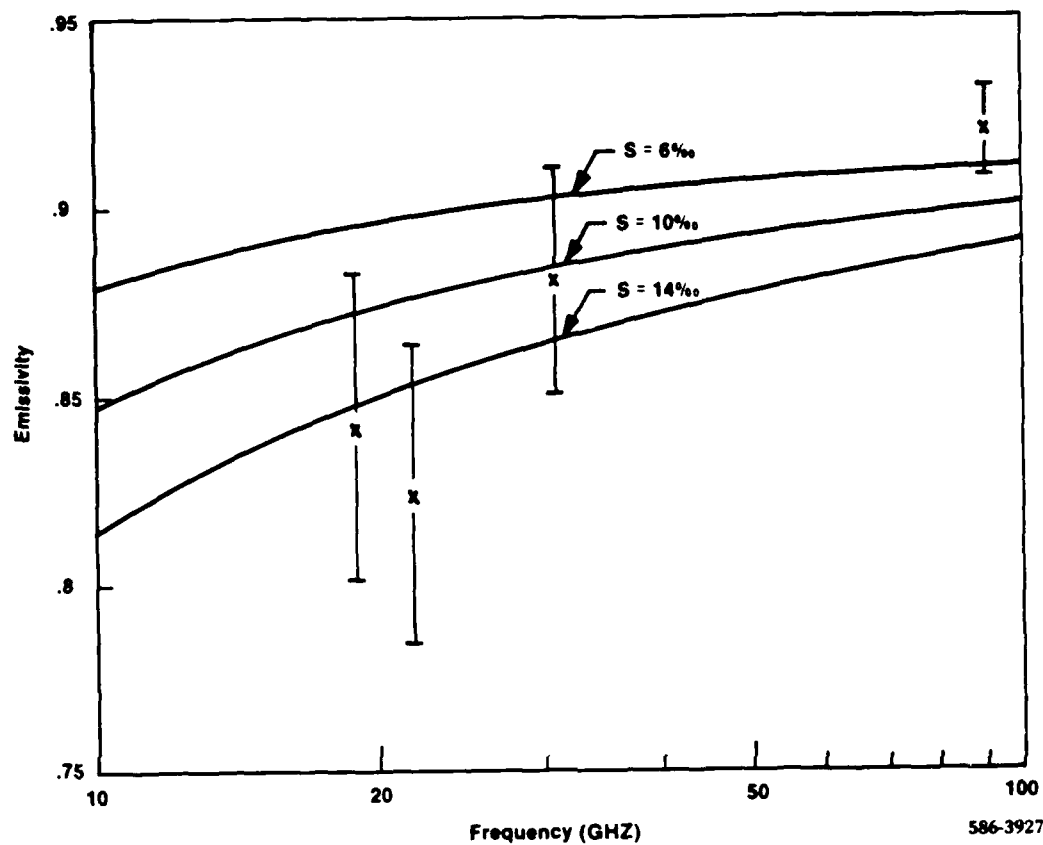
Figure 2-3. Emissivity of Snow Free New Ice as a
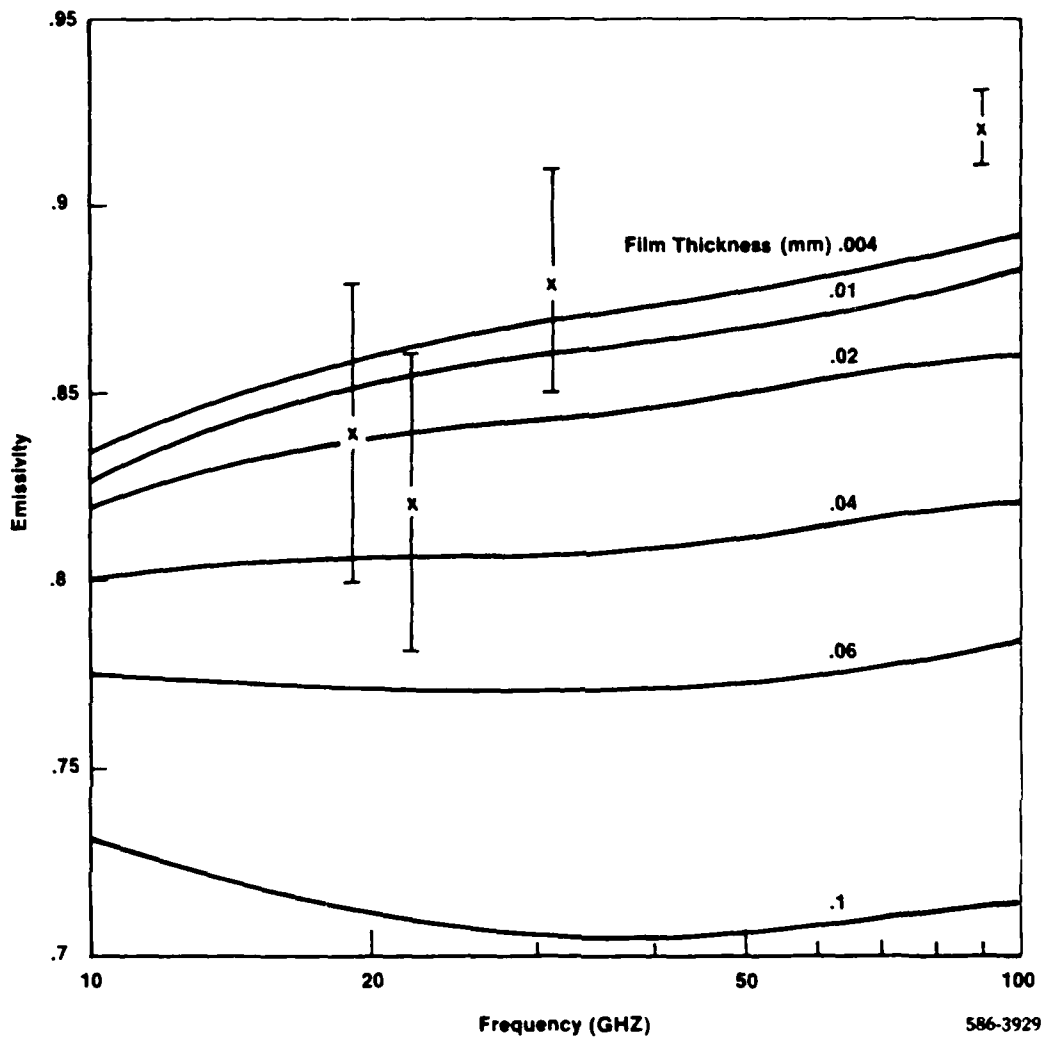Function of Frequency for

$\theta = 0°$ ($T_g = 270$ K, $\rho = .85$ g/cm^3)
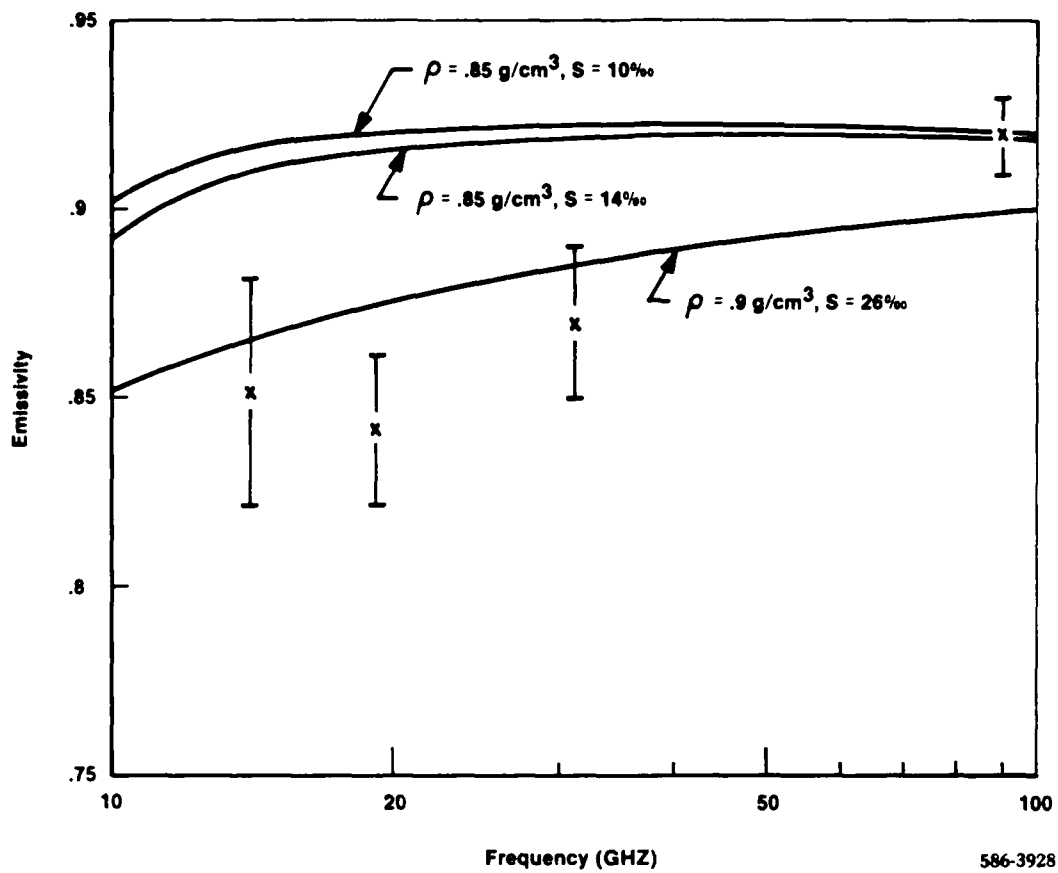
Figure 2-4. Emissivity of Snow Free New Ice as a
Function of Frequency for

$\theta = 0°$ (T_g = 263 K)

Figure 2-5. Emissivity of New Ice Covered with

a Film of Brine for

$\theta = 0°$ (T$_g$ = 270 K, S = 10^0/oo, ρ = .9 g/cm3)
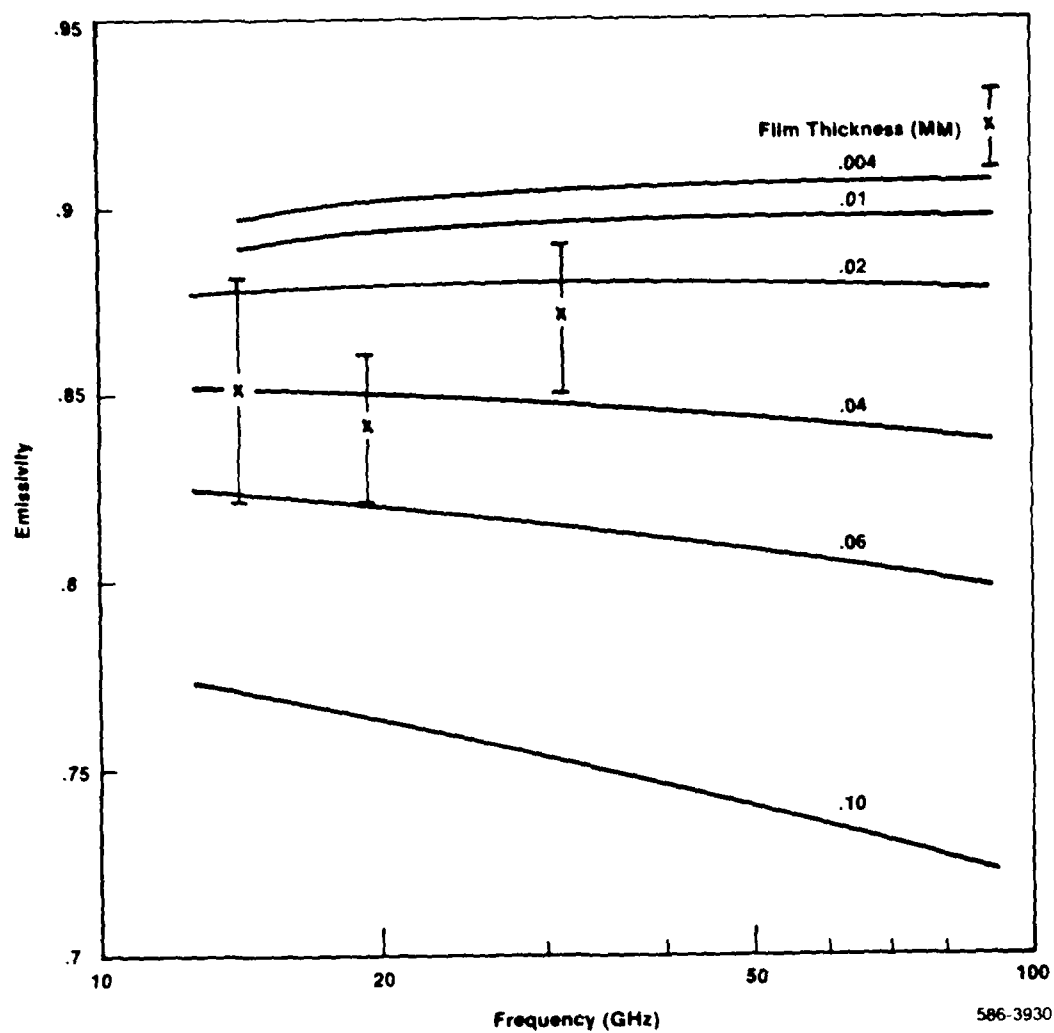
Figure 2-6. Emissivity of New Ice Covered with
a Film of Brine for

$$\theta = 0° \ (T_g = 263 \ K, \ S = 10.3°/oo, \ \rho = .9 \ g/cm^3)$$
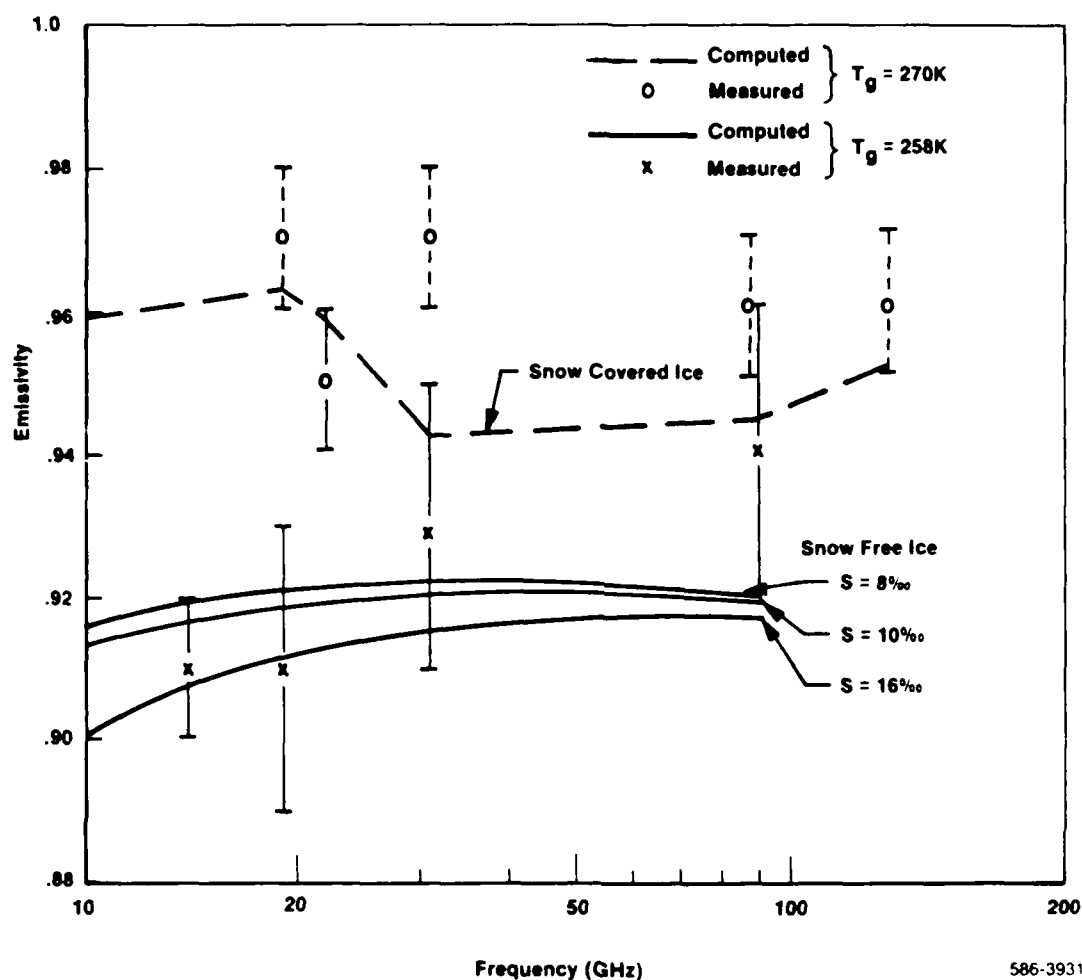
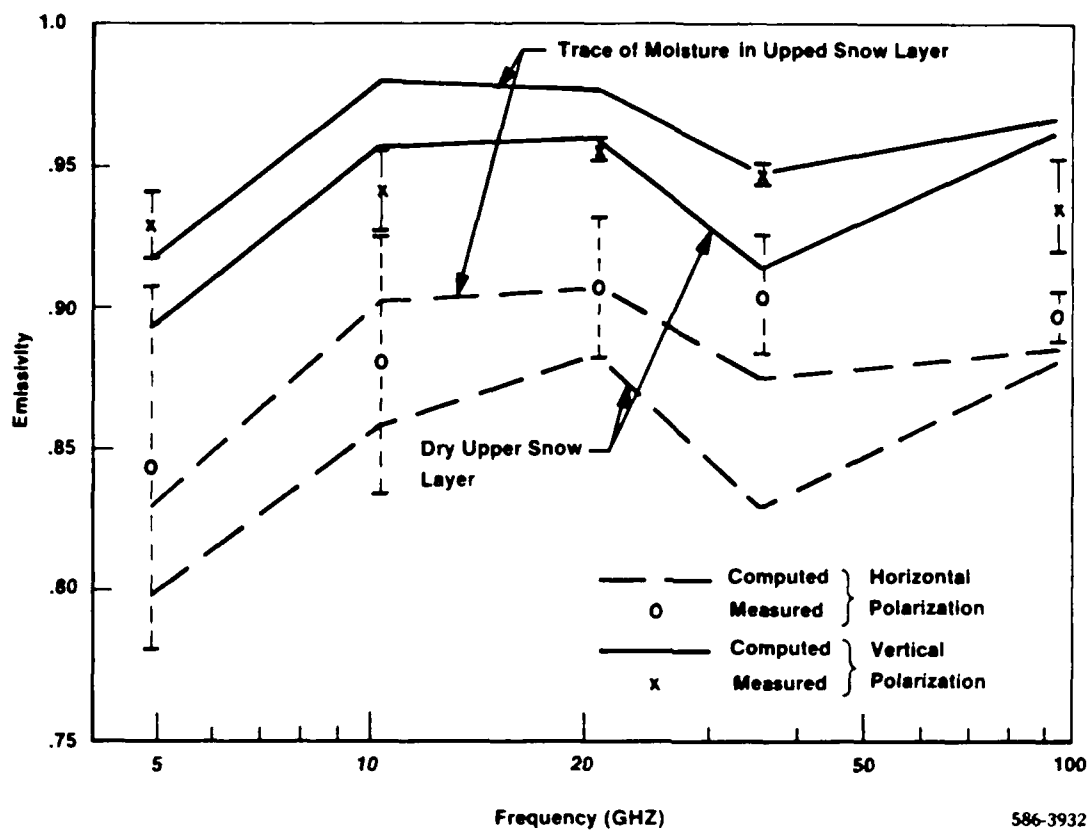Figure 2-7. Emissivity of Young Ice as a Function of
Frequency at $\theta = 0°$

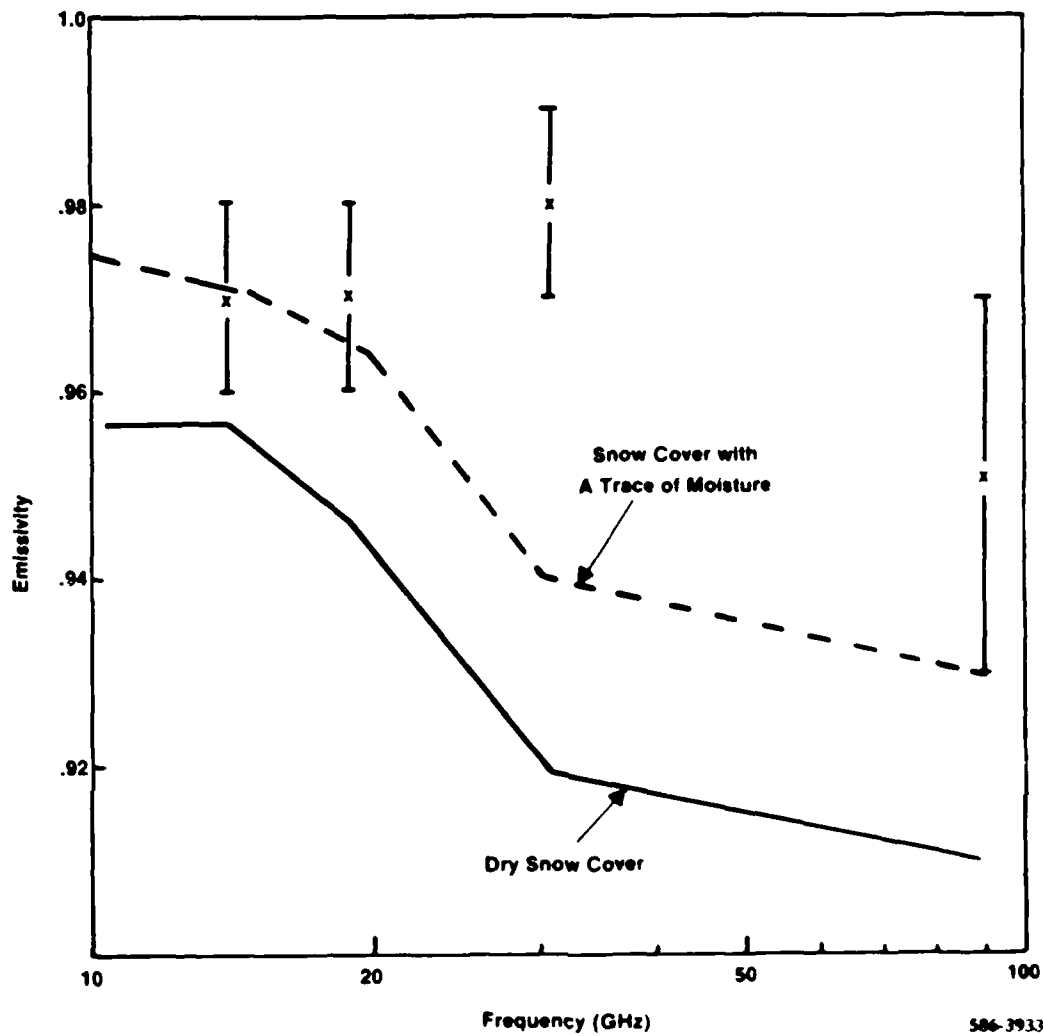Figure 2-8. Emissivity of First-Year Ice as a Function of Frequency at $\theta = 50°$ ($T_g = 272$ K)

Figure 2-9. Emissivity of First-Year Ice as a Function of
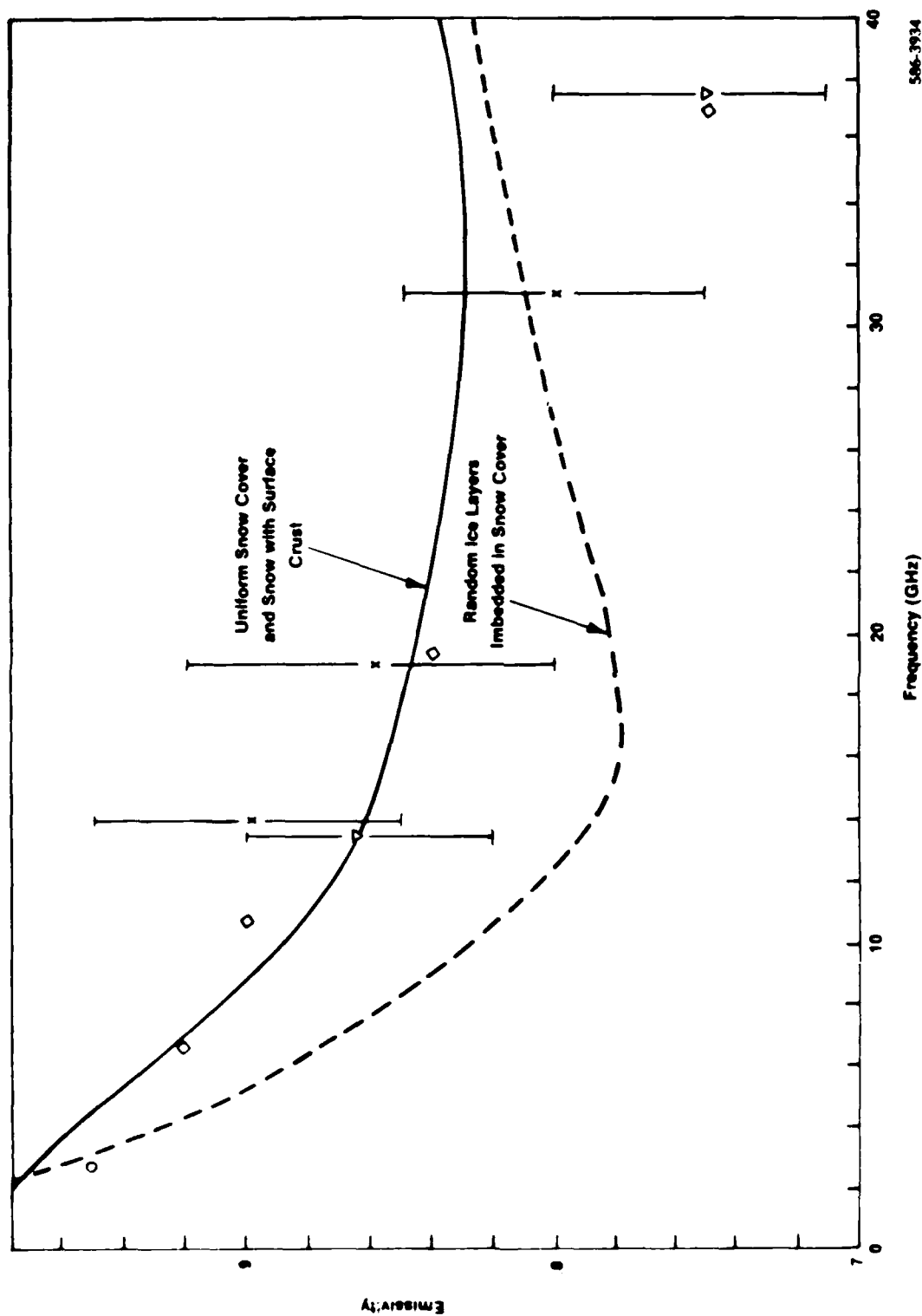Frequency for $\theta = 0°$ ($T_g = 253$ K)

Figure 2-10. Emissivity of Multi-Year Ice as a Function of Frequency for $\theta = 0^\circ$ ($T_g = 253$ K)
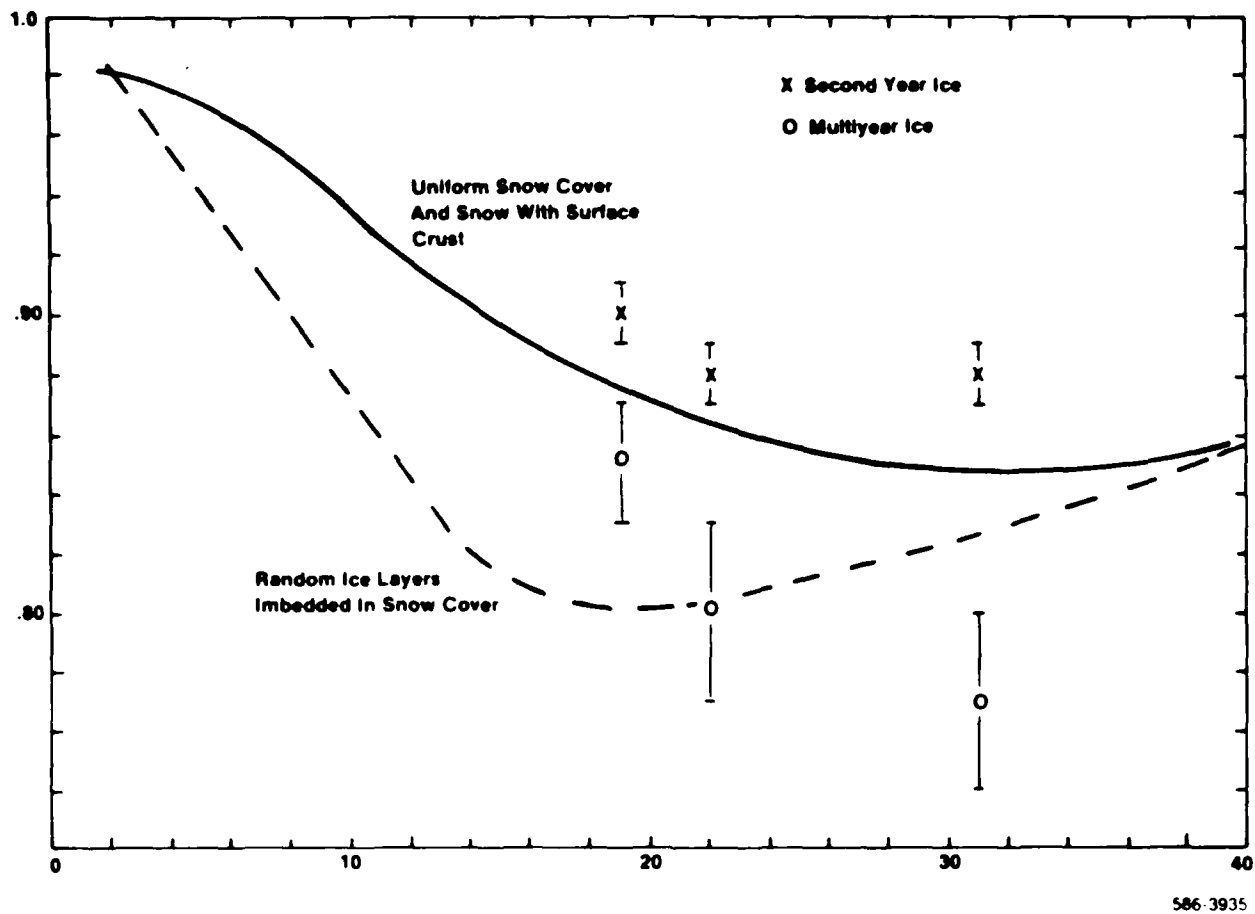
S86-3935

Figure 2-11. Emissivity of Multiyear Ice as a Function of

Frequency for $\theta = 0°$ (T_g = 270 K)

Section 3

CONCLUSIONS AND RECOMMENDATIONS

A theory of the microwave brightness temperature of sea ice based on the bilocal approximation in strong fluctuation theory has been developed and shown to be able to account for reported measurements on new, young, and first-year sea ice over a variety of temperature conditions and frequencies up to 140 GHz. Experimental data on multiyear ice are explainable at low frequencies, but the theory begins to become less quantitatively correct in the 20-30 GHz range. Calculations for multiyear ice at higher frequencies do not accurately reproduce measurements.

The theory shows that snow cover on sea ice has a significant effect on its emission characteristics and is responsible for the differences in the observed spectral signature of new and young ice without snow cover compared to young ice with snow cover and first-year ice (which almost always is covered with snow). The effect of snow is not only to increase the emissivity of these types of sea ice but also to flatten the spectral curve so that the emissivity becomes almost independent of requency. For these reasons, young ice (which may or may not have snow cover) can appear to be radiometrically either like new or first-year ice. This has been observed in the literature. Also, for these ice types, where the salinity is high, it appears that salt from the ice can infiltrate the bottom-most layer of snow and cause the appearance of some free water in the snow even though the temperature may be quite low.

For snow-free ice, a model with a film of water on the ice surface was investigated. This model has been suggested in the literature to explain

certain features of the microwave signature (which can also be explained on the basis of a higher bulk salinity). It was found that the required film thickness is very small - no more than 20 to 30 micrometers. This is, perhaps, too small to be reasonable so that such a model may not be plausible. In addition, it does not reproduce high frequency (90 GHz) data as well as models without the film. Because the explanation of published data does not actually require such a hypothesis, it was rejected in this study.

The principal difficulty with the theory appears to be in accounting for the high frequency (above 30 GHz) decrease in the emissivity of multiyear sea ice. A possible cause for this problem may lie in the fact that the loss tangent of pure ice (as it exists in the ice grains of the snow cover) is incorrectly specified and thus leads to a poor estimate of scattering effects in the snow and its consequent influence on the ice emissivity. The lack of knowledge concerning the dielectric constant of pure ice has been pointed out in previous studies. Another, possibly more significant, reason for the failure to predict the small emissivity of multiyear sea ice at high frequencies is the fact that the bilocal approximation in strong fluctuation theory ignores second and higher order terms in a perturbation expansion of the random field scattered by the inhomogeneities of the medium. The reduced scattering implies a higher emissivity. At lower frequencies, where scattering may be adequately treated by keeping only the leading term, the theory was able to reproduce the experimental data quite well. Thus, the development of a method for including higher order scattering corrections should receive high priority.

On the experimental side, this study has shown that ice conditions such as density and salinity gradients within the first few centimeters of the surface (or ice-snow boundary) may be quite important. Yet, almost no experimental data is available on this subject. Much more attention should be paid to this area in studies related to microwave radiometry. Also, the question of whether future models should consider possible water films on the ice depends on measuring a film of water only a few tens of micrometers thick. Tentatively, this model has been rejected, but a definitive decision requires more data. Finally, an extremely important area from the point of view of radiometric studies is a full description of any snow cover on the ice. Descriptions of this nature have almost never appeared but, as this study has shown, the snow cover is very significant. Whether it is dry or wet, uniform or multilayered with embedded ice layers, thick or thin can have an important role in the interpretation, computation, and, ultimate achievement of a full understanding of sea ice emissivity. Of course, to obtain such data requires ground truth data that is often not available when aircraft or satellite overflight of ice are made. However, as at least one example in this study has shown, such data can be very valuable so that occasional supporting ground parties should be fielded to support these remote experiments.

END

4-87

DTIC